RICE UNIVERSITY

Water-phase Synthesis of Cationic Silica/polyamine Nanoparticles
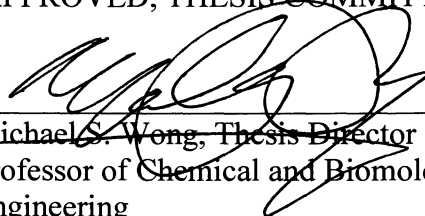
by

Quang Xuan Luong Nguyen

A THESIS SUBMITTED
IN PARTIAL FULFILLMENT OF THE
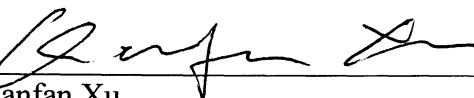REQUIREMENTS FOR THE DEGREE

Master of Science

APPROVED, THESIS COMMITTEE:

Michael S. Wong, Thesis Director
Professor of Chemical and Biomolecular
Engineering
Professor of Chemistry

Junichiro Kono, Chair
Professor of Electrical and Computer
Engineering

Qianfan Xu
Assistant Professor of Electrical and
Computer Engineering

Pulickel M. Ajayan
Benjamin M. and Mary Greenwood
Anderson Professor in Engineering
Professor of Mechanical Engineering and
Materials Science

HOUSTON, TEXAS
DECEMBER 2011

ABSTRACT

Water-phase Synthesis of Cationic Silica/polyamine Nanoparticles

By

Quang Xuan Luong Nguyen

Functionalizing surfaces with amine groups through the hydrolytic condensation of aminotrialkoxysilanes is a typical approach when modifying silica particles for use in bioimaging, enzyme immobilization, and other applications. This processing step can be eliminated if amine-functionalized silica particles are directly prepared without using aminotrialkoxysilanes. Here, a one-pot, ambient-condition, water-phase method to synthesize silica-based nanoparticles (NPs) that present surface amine groups is described. The formation mechanism involves the electrostatic crosslinking of cationic polyallylamine hydrochloride by citrate anions and the infusion of the formed polymer/salt aggregates by silicic acid. The particles were unimodal with average diameters in the range of 40 to 100 nm, as determined by the size of the templating polymer/salt aggregates. Colorimetric analysis using Coomassie brilliant blue and zeta potential measurements confirmed the presence of surface amine groups of the hybrid silica/polymer NPs. Surface charge calculations indicated the hybrid NPs had a lower amine surface density than aminopropyltriethoxysilane-functionalized silica (0.057 #/nm^2 vs. 0.169 #/nm^2 at pH 7).

Acknowledgements

I would like to thank my advisor, Dr. Michael Wong, for providing guidance, insights, and resources which made this thesis possible.

I would not be this far along my academic path without encouragements and support from Dr. Sakai Tomokazu, Dr. C.N. Chinnasamy, Dr. Vincent G. Harris from Northeastern University and Dr. Seth Fraden from Brandeis University. Without your guidance and help late in my undergraduate career, I would not be working in this exciting field of nanotechnology.

I have to say that the Wong group members are the greatest bunch of people I've ever worked with. I want to personally thank Nikolaos Soultanidis, Gautam Kini, Lori Pretzer, Sravani Gullapalli, Juan Velazquez, Hitesh Bagaria, and Shyam Benegal for providing help whenever I need, provide jokes whenever things are not going well, and making my time at Rice so much more enjoyable.

Lastly, I would not be where I am today without my parents, brother, aunts, uncles, relatives, who have given their full support in whatever endeavors I strive for. You provided everything for me and I can never repay back. And PhiSon Le, what would I ever do without you.

Table of Contents

List of Figures

List of Tables

Chapter 1

Introduction

1.1 Silicon Basics

Silicon is considered to be among the most important elements in the periodic table. It is the second most abundant element on Earth making up 27.7% of the Earth's crust and is second to only oxygen.[1] There is speculation among silicon researchers that silicon, specifically silica, may have had an integral role in the formation of life on Earth. This speculation comes from the fact that diatoms, the simplest form of unicellular algae found in all bodies of water on Earth, utilized silicon precursors to form a silica shell for protection of their inner essential parts.[2-4] The fact that silicon can have up to four covalent bonds similar to carbon supports this speculation. Its importance is not limited to the evolution of life on Earth; silicon played a crucial role in the advancements made in electronic technology in the 20th century with its semiconducting properties. A semiconductor is a material that can conduct or insulate electrical currents depending on its form, in this case, crystalline silicon (conductor) or silicon dioxide (insulator). Crystalline silicon is mostly used in the semiconductor industry, whereas, silicon dioxide found its way for other kinds of applications.

1.2 Applications for Silica Nanostructures & Mesostructures

Silica, or silicon dioxide (SiO_2), is highly utilized for its applications at the macroscale level. The basic unit of silica, monosilicic acid (SiO_4), has a tetrahedral structure as in Figure 1-1a and these units can combine into different states: amorphous

or crystalline (Figure 1-1b). Crystalline silica can be classified into several distinct structures: α and β forms of quartz, tridymite, cristobalite, among others.[5] Amorphous silica was manufactured into several forms: fused quartz, fumed silica, silica gel, aerogel, and colloidal silica. Previously, amorphous silica was limited to macroscale applications such as cement densifier, moisture absorbents, and stabilizing agents, among others. Recent development in synthesizing colloidal silica at the microscale level has extended its applicability to the biomedical field.
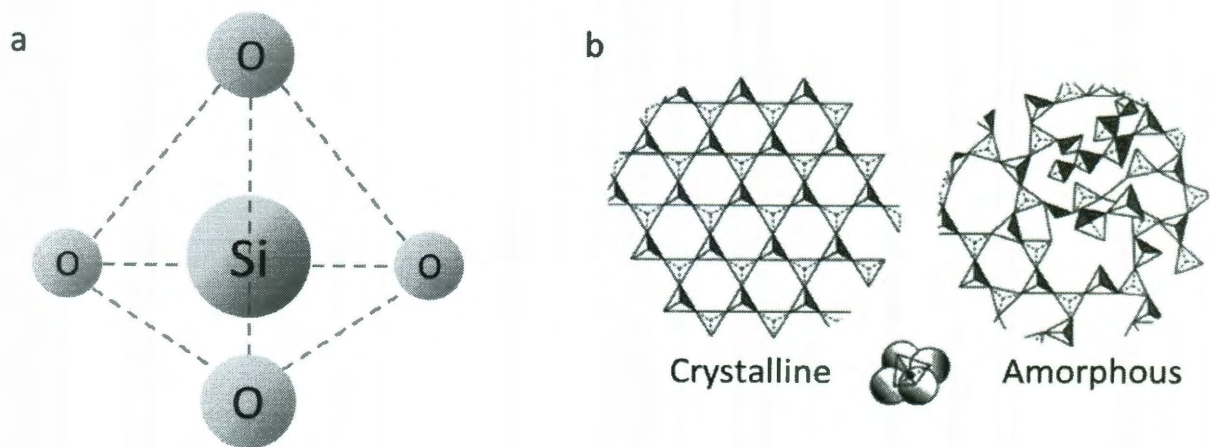
Figure 1-1. a) The basic unit of silica with a tetrahedral structure. b) Crystalline and amorphous formation of silica.[6]

Colloidal silica particles have been successfully synthesized into smaller size nanoparticles (1-100 nm) and mesoparticles (100-1000 nm). These sub-micrometer particles are a major component in cosmetics, surface coatings, food additives, among others. Since its existence is everywhere, its potential toxicity must be addressed. The most common exposure to crystalline silica is the inhalation in dust or powder form, which is hazardous over time and can lead to diseases such as silicosis, pulmonary tuberculosis, or lung cancer. These diseases are caused by lodged dust silica in the lung,

decreasing its capability to extract oxygen from the air. Prolonged exposure to dust silica with levels higher than 0.1 mg/m^3 increase the risk for lung damage.[7] Asbestos is another crystalline silica-based material that is a well-known health hazard. It is a silicate mineral with long and thin fibrous characteristics that was used widely in buildings for its fire-retardant and insulation properties.[8] Unlike its crystalline form, amorphous silica was determined to not cause silicosis or other lung diseases. Amorphous silica is considered to be "low toxicity" by the CDC, but prolonged inhalation can cause irreversible false x-ray readings of the lung without disabling its oxygen extraction functionality.[9] The World Health Organization (WHO) confirmed that ingestion of amorphous silica is harmless. In fact, food such as potatoes, milk, and drinking water contains 10.1, 2.1, and 7.1 μg silica per gram, respectively. [10] This makes silica of great interest for applying silica to biological applications.

1.3 Background on Silica-Hybrid

Colloidal silica particles are categorized into three different classes: inorganic silica, organosilica, or multi-silicate. Inorganic silica synthesis consists of either precursors: tetraethoxyorthosilicate (TEOS) or tetramethoxyorthosilicate (TMOS). TEOS and TMOS are frequently used silica precursors because their tetrahedral structure (center Si with 4 O surrounding) form simple silica networks (–O–Si–O–) without residue of any other elements. TEOS and TMOS structures are shown in Figure 1-2a-b. The terminating end of these simple silica colloids are mainly silanol groups (–Si–OH). For a different termination of the silica colloids, organosilicate should be used as

precursor as opposed to TEOS and TMOS.   This modified silica is classified as

organosilica. [2, 11-13]

a

tetramethoxyorthosilicate
(TMOS)

b

tetraethoxyorthosilicate
(TEOS)

c

octyl triethoxysilane
(OTES)

d

vinyl triethoxysilane
(VTES)
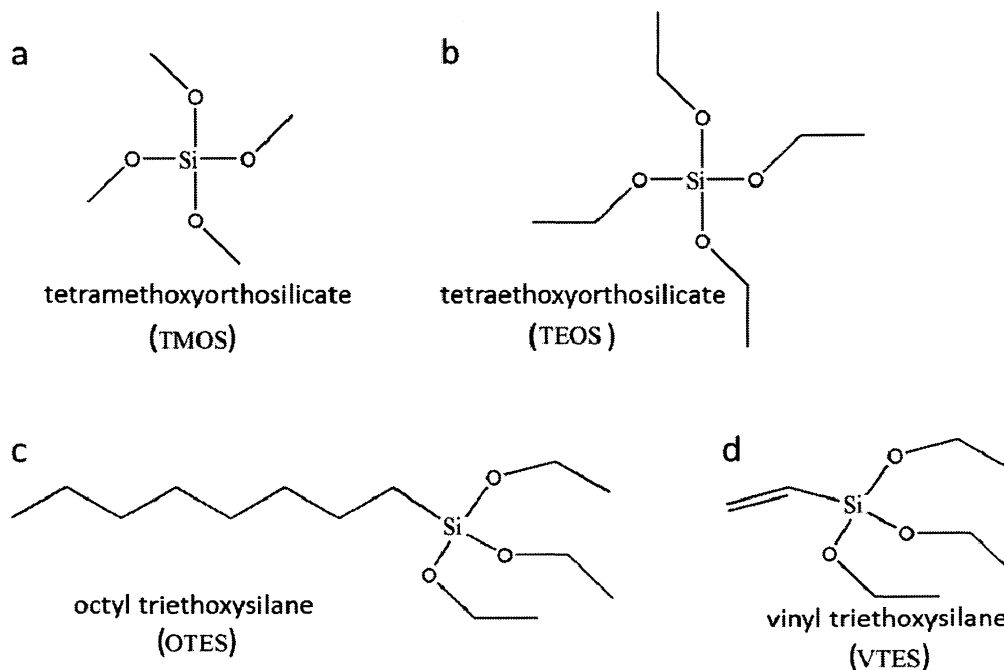
Figure 1-2. Typical precursors for silica synthesis with a-b) classified toward inorganic
while c-d) are considered organosilica.

Organosilica is further broken into two subcategories: organically modified silane

(ORMOSIL) or functional organosilica. The main difference between organosilica and

inorganic silica is the inclusion of organic content within its structure. ORMOSIL has

carbon chains and carboxylic surface groups in its chemical structure. Commonly used

precursors to synthesize ORMOSIL are octyl triethoxysilane (OTES) and/or vinyl

triethoxysilane (VTES) (see Figure 1-2 c-d).   Functional organosilane consists of

additional thiol or epoxide groups along the carbon chains.   The resulting particle

synthesis using these precursors has a surface functionalized with both carboxyl and

either thiol or epoxide groups. Precursors for functional organosilica include 3-mercaptopropyltrimethoxysilane (MPMS) and 2- (3, 4-Epoxycyclohexyl)ethyltrimethoxysilane (EpoMS). As the name suggests, multi-silicate is a combination of inorganic silica or organosilica with other silicon precursors to achieve multifunctional groups within its structure. [14]

1.4 Biomimetic Synthesis of Silica

Diatoms have utilized silicon precursors (found in nature) to synthesize their silica shell since the beginning of their existence approximately 190-200 million years ago.[15] A sample of several diatom structures are shown in Figure 1-3. Diatoms are believed to share ancestry with heterokonts,[16] a group of protists (eukaryotic microorganisms) whose existence date back to approximately 725 million years ago.[17, 18] Silica compounds used by diatoms are identified as either metasilicic acid ($SiO(OH)_3^-$) or orthosilicic acid ($Si(OH)_4$). The exact process of silicic acid polymerization to silica and the delivery of silica to the cell wall within the diatom is unclear, however, silica shell formation after absorption into the diatom's internal structure is known. Silicic acid is brought into the silica deposition vesicle (SDV) through Na^+ proteins, also known as the silicic acid transporters (SITs) [22]. Once absorbed by SDV, the silicic acid assumes the form of metasilicic acid.[9, 24]. Metasilicic acid hydrolyzes to form dimers, trimers and so forth, called polysilicic acid. Polysilicic acid is then deposited onto fustulins, pleuralins, or silaffins- highly hydrophilic proteins that are bounded to the cell wall. The latter protein contains oligo-N-methylpropylamine units that were found to catalytically promote polysilicic acid precipitation to silica. Silica is then deposited into spaces

between protonated and unprotonated amine groups.[25] Polysilicic acid fills in the gap between the sites of amine-bound silica to form the diatom shell. Diatoms come in all shapes and sizes in the 1-100 μm range with shell thickness being several hundred nanometers.

Figure 1-3. Scanning electron microscopy of diatoms in various shapes and sizes.[19]

1.5 Conventional Silica Particles Synthesis

The majority of silica particles adapted for biological applications are inorganic and can be achieved by using a modified Stöber method. Monodispersed colloidal silica spheres were first synthesized in 1968 by Stöber et al.[20] Briefly, tetraalkyl silicates are added into a well-mixed solution of alcohol, ammonia, and deionized water and stirred for 120 minutes. The size of the silica colloidal sphere is controlled by varying the ratio of alcohol to ammonia. The Stöber method was able to produce silica particles with diameters ranging from 0.05-1.68 μm with relative standard deviation (RSD) < 10% for all samples as seen in Figure 1-4a, which made these particles to be considered "narrow" monodispersed.[21] Further improvements to this method by 1) varying the ammonia:

6

alcohol: deionized water ratio, 2) controlling the stirring speed and 3) reaction temperature, produce silica diameters as small as 20 nm (Figure 1-4b).[22-25]
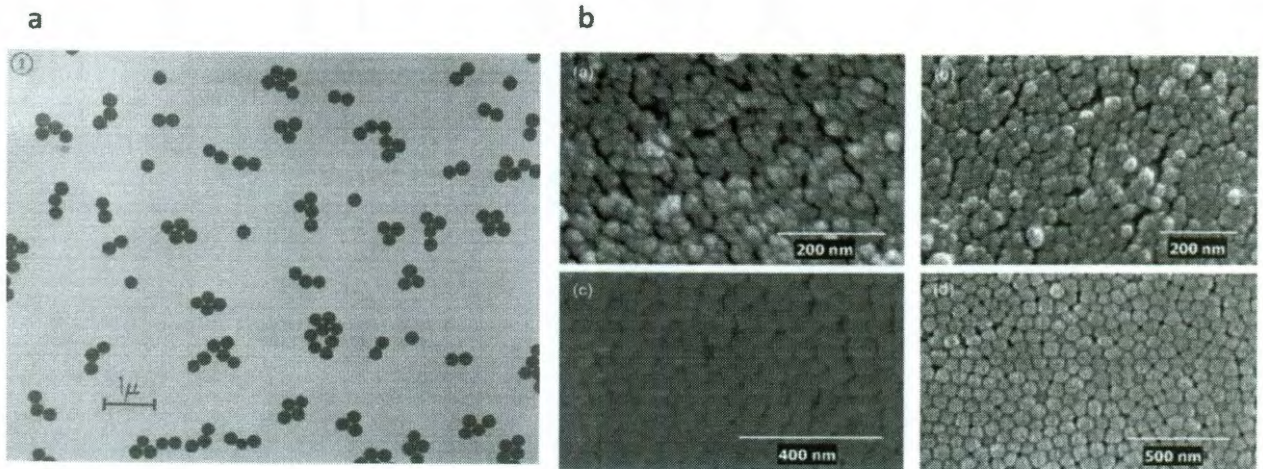
Figure 1-4. a)Silica particles synthesized by Stober[20] and b) smaller diameter particles using a modified method.[25]

The surface groups on inorganic, colloidal, silica spheres are inefficient in linking with dyes, DNAs or other particles. There are two approaches to make the surface groups more suitable for the desired applications: 1) start with pre-functionalized organosilane silica as the base[26, 27] or 2) functionalize the surface of inorganic silica.[28-34] The latter method is used more frequently due to the commonality and simplicity in the Stober method. Examples of linker molecules for different surface group functionalization are aminopropyltriethoxysilane (APTES) or aminopropyltrimethoxysilane (APTMS) for amine groups, or mercaptopropyltrimethoxysilane (MPTES) for thiol groups. Applying the linker molecules to the surface requires stirring overnight and slight heating of the solution to ensure a tighter packing density. Another way to change the surface groups is by adding positively charged molecule/polymers so that it can stick onto the surface by

electrostatic forces. Subsequently, inversely charged polymers/molecules can be added to further change the surface groups.This method is known as the layer-by-layer (LbL) method.[35]

1.6 Nanostructure and Mesostructure Formation from Polymer

Cationic polyallylamine is mentioned frequently in many layer-by-layer (LbL) syntheses for thin films or surface functionalization; however, it is not as frequently applied for nanoparticle synthesis. For a typical synthesis of nanoparticles <10nm using nanopores created from polyelectrolyte (PE) multilayer film (layers of oppositely charged polyallylamine hydrochloride (PAH) and polyacrylic acid (PAA)), metal precursors are added followed by a reducing agent to form the desired nanoparticles. Examples of this method for synthesizing silver nanoparticles with average sizes ranging from 4-8nm [36] and ZnS having average size 3-4nm [37] are shown in Figure 1-5a.
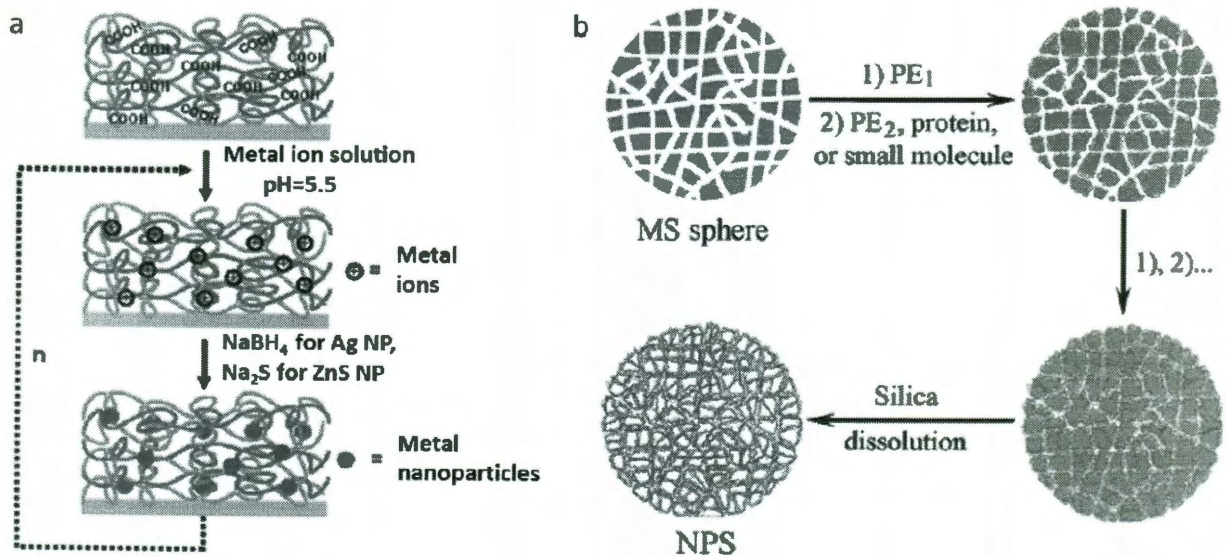
Figure 1-5. Scheme of synthesis of a) Ag, ZnS nanoparticles[36, 37] and b) polyelectrolyte microparticles.[38]

Besides the LbL method, PAH can also be a precursor for polymer particles. Taking advantage of mesoporous silica particles as a template, Figure 1-5b shows the scheme for the addition of oppositely charged PAA and PAH followed by dissolution of silica to produce nanoporous, spherical, polymeric particles (1.2 - 1.9 μm).[6] These particles are found to have a high capacity for immobilization of proteins. PAA is not the only anionic polymer that can be used to complement PAH for formation of polymeric particles. To get smaller size polymeric particles, anionic salt has to be used as the cross-linking agent.

Cationic polymer and multivalent anionic salt form spherical aggregates with high stability and monodisperse distribution. Sumper et al. showed that cationic polyamines, from diatoms, formed silica mesoparticles in the presence of anionic phosphates and followed by the addition of silicic acid. [39-41] Expanding from that work, nanoparticle-assembled capsules (NACs) were formed by combining poly(L-lysine) (PLL) with anionic salts such as ethylenediamine (EDTA) or citrate salt resulting in cationic colloidal aggregates as core templates. 12nm anionic silica nanoparticles, attracted to the colloidal aggregate by electrostatic charge, envelop the aggregate template resulting in the core shell structure of NACs.[42] Further study of colloidal aggregate formation was performed by changing the anionic salt. Trivalent citrate was found to promote polymer aggregation over a larger range of concentrations (Figure 1-6b) compared to tetravalent EDTA (Figure 1-6a) and divalent succinate (Figure 1-6c). Also, no polymer aggregate formation was found for monovalent acetate (Figure 1-6d).
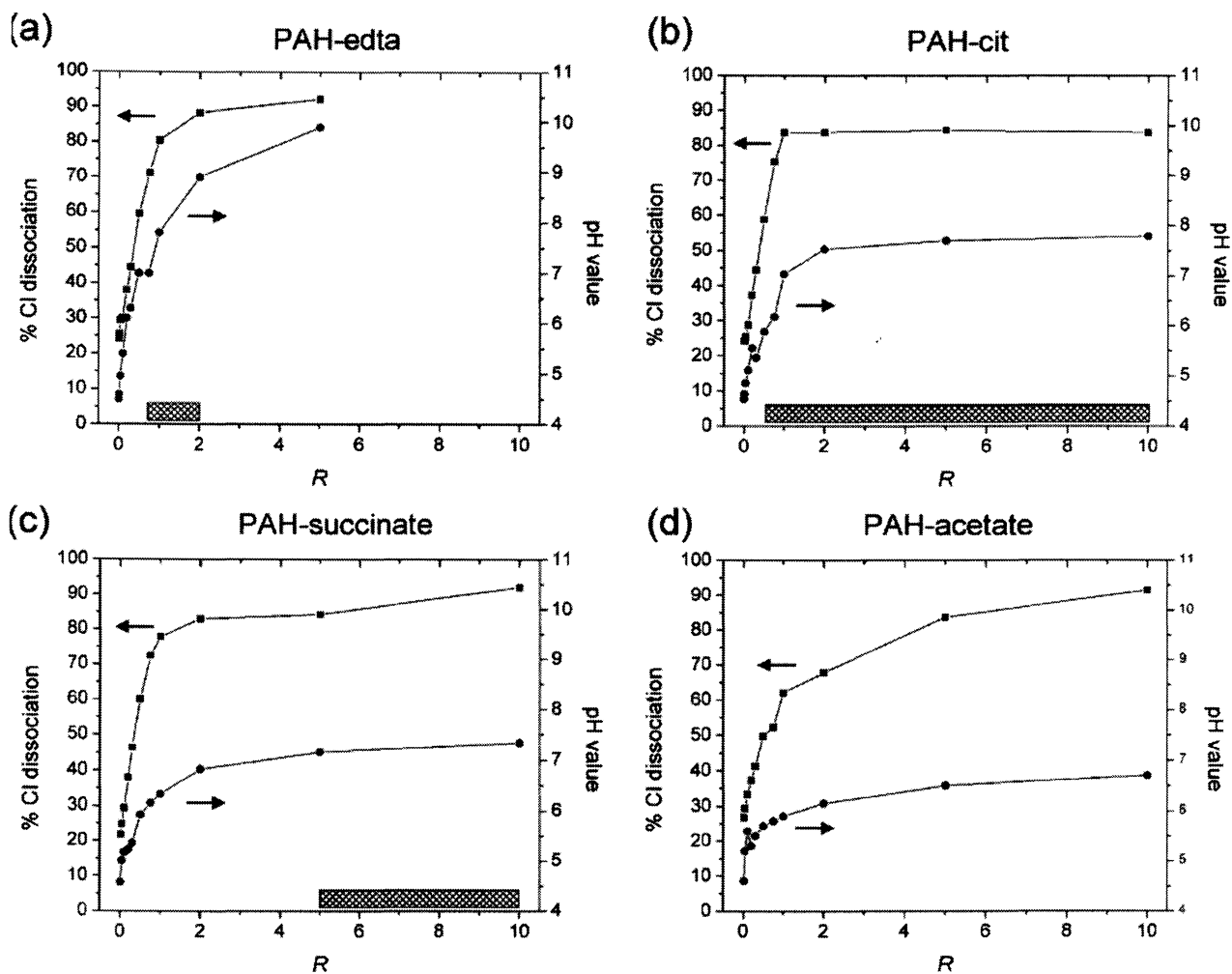
Figure 1-6. Cl dissociation plot of PAH and corresponding pH values. The R on the x-axis represent the charge ratio of anion to cation. Gray area represents colloidal aggregates formation from cationic polyamines and anionic a) EDTA, b) citrate, c) succinate, and d) acetate. The wider range of charge-ratio for PAH-cit plot allows more flexibility in forming aggregates.[43]

Murthy et al. also showed that colloidal aggregates less than 100 nm in size are formed if the charge ratio of anions to cations is low enough.[43] Bagaria et al recently showed that adding silicic acid to NACs increases the shell thickness.[44] The shell thickens inwardly by diffusing through the silica nanoparticle shells solidifying the PAH-citrate core without increasing the overall size of the NACs. We want to investigate the formation of silica hybrid nanoparticles through the use of silicic acid.

1.7 Silicification of PAH-citrate Particles

Although polymer salt aggregate (PSA) derived silica nanoparticles is not as complex as the diatom biological system, there are many similarities in which the two systems silicize particles. Deriving from the functionality of SDV within the diatom, one of the steps toward silicification for our PSA is by the aid of Na^+ ion from sodium tricitrate precursor. The Na^+ promotes the instability of silicic acid/ SiO_2 suspension. The next step to consider is the deposition step within the PSA. PAH is known for its high amine density, therefore it provides numerous sites for deposition. With numerous sites deposited by silica in close proximity, polymerization is highly promoted and in our case, formation of solid silica-hybrid nanoparticles that assume the size of their PSA template.

1.8 Motivation

Organic-silica hybrid nanoparticles and submicron particles are of great interest for a wide variety of applications including optics[45], non-viral vectors for genetic therapy[11], enzyme immobilization[46], coatings[47], bioimaging, drug delivery, sensing, and therapeutics[48]. Currently used approaches for silica particle formation include hydrolytic and non-hydrolytic sol-gel syntheses, mini-emulsion polymerization, and biomimetic chemistry.[20, 39-41, 49-56] A new chemistry route to silica hybrid particles is desirable if the processing steps can be simplified or eliminated while still yielding particles of controlled size and uniformity in the more difficult range of sub-100 nm.

In this study, we report the ambient-condition, water-phase synthesis of silica/polyamine hybrid particles in the sub-100-nm range using PSA assembly chemistry. The PAH and citrate anion charge ratio was studied for its effect on the hydrodynamic diameter of the resultant PAH-citrate aggregates. After the addition of silicic acid, the formed silica/PAH hybrid NPs were characterized for particle size, zeta potential, and organic content. These NPs are unimodal, with relative standard deviations in the 15-20% range. They are also positively charged due to the presence of PAH amine groups exposed at the particle's surface with surface charge properties between those of pure silica NPs and aminoalkylsilane-functionalized silica mesoparticles.

1.9. References

1. Monroe, J.S., R. Wicander, and R.W. Hazlett, *Physical geology: exploring the Earth*. 2007: Thomson Brooks/Cole.
2. Bauerlein, E., *Biomineralization: progress in biology, molecular biology and application*. 2nd ed. 2004: Wiley-VCH.
3. Hildenbrand, M., ed. *Silicic Acid Transport and Its Control* Biomineralization, ed. E. Bauerlein. 2000, Wiley-VCH: Weinheim, FRG. 171-188.
4. Iler, R.K., *The Chemistry of Silica*. 1979: John Wiley & Sons, Inc.
5. Wiberg, E., N. Wiberg, and A.F. Holleman, *Inorganic chemistry*. 2001: Academic Press.
6. Bergna, H.E. and W.O. Roberts, eds. *Colloidal Silica: Fundamentals and Applications*. Surfactant Science. 2006, CRC Press.
7. Cee, R., et al. *Silica and Silicosis*. 1996 [cited 2011 7/14].
8. Alleman, J.E. and B.T. Mossman, *Asbestos Revisited*. Scientific American, 1997(7): p. 70-75.
9. Control, C.f.D., *Occupational Health Guideline for Amorphous Silica*, U.S.D.o.H.a.H. Service, Editor. 1978: Washington, D. C. p. http://www.cdc.gov/niosh/topics/silica/.
10. Additives, J.F.W.E.C.o.F., *WHO Food Additives Series No. 5*, in *FAO Nutrition Meetings Report* 1974: Geneva.
11. Bharali, D.J., et al., *Organically modified silica nanoparticles: A nonviral vector for in vivo gene delivery and expression in the brain*. Proceedings of the National Academy of Sciences of the United States of America, 2005. **102**(32): p. 11539-11544.
12. Yamanaka, J., et al., *Control of the surface charge density of colloidal silica by sodium hydroxide in salt-freeand low-salt dispersions*. Physical Review E, 1997. **55**(3): p. 3028-3036.
13. Hunter, R.J., *Foundations of Colloids Science*. 2001, New York: Oxford University Press.
14. Nakamura, M., ed. *Approaches to the Biofunctionalization of Spherical Silica Nanomaterials*. Nanostructured Oxides, ed. C.S.S.R. Kumar. Vol. Nanomaterials for the life sciences. 2009, Wiley-VCH.
15. Smol, J. and E. Stoermer, *The Diatoms: Applications for the Environmental and Earth Sciences*. 2010: Cambridge University Press.
16. Leedale, G.F., *How Many Are the Kingdoms of Organisms?* Taxon, 1974. **23**(2-3): p. 261-270.
17. Medlin, L.K. and I. Kaczmarska, *Evolution of the diatoms: V. Morphological and cytological support for the major clades and a taxonomic revision*. Phycologia, 2004. **43**(3): p. 245-270.
18. Yoon, H.S., et al., *A Molecular Timeline for the Origin of Photosynthetic Eukaryotes*. Molecular Biology and Evolution, 2004. **21**(5): p. 809-818.
19. Microscopy, C.f.A. Scanning Electron Micrographs 2007 [cited 2011 Mar 4].

20.   Stöber, W., A. Fink, and E. Bohn, *Controlled growth of monodisperse silica spheres in the micron size range.* Journal of Colloid and Interface Science, 1968. **26**(1): p. 62-69.

21.   Yu, J., et al., *Self-assembly synthesis, tumor cell targeting, and photothermal capabilities of antibody-coated indocyanine green nanocapsules.* J Am Chem Soc, 2010. **132**(6): p. 1929-38.

22.   Chen, S.-L., P. Dong, and G.-H. Yang, *The Size Dependence of Growth Rate of Monodisperse Silica Particles from Tetraalkoxysilane.* Journal of Colloid and Interface Science, 1997. **189**(2): p. 268-272.

23.   Chen, S.L., Colloids Surf. A, 1998. **142**(1): p. 59-63.

24.   H. C. Wang, C.Y.W., C. C. Chung, M. H. Lai, T. W. Chung, Ind. Eng. Chem. Res., 2006. **45**(24): p. 8043-8048.

25.   Huang, Y. and J.E. Pemberton, *Synthesis of uniform, spherical sub-100 nm silica particles using a conceptual modification of the classic LaMer model.* Colloids and Surfaces A: Physicochemical and Engineering Aspects, 2010. **360**(1-3): p. 175-183.

26.   Goldbaum, E. *Using nanoparticles, in vivo gene therapy activates brain stem cells.* Medical News Today 2005 [cited 2011 July].

27.   Duarte, F.J., *Solid-state multiple-prism grating dye-laser oscillators.* Appl. Opt., 1994. **33**(18): p. 3857-3860.

28.   Botella, P., et al., *Surface-modified silica nanoparticles for tumor-targeted delivery of Camptothecin and its biological evaluation.* Journal of Controlled Release, 2011. **In Press, Uncorrected Proof**.

29.   Howarter, J.A. and J.P. Youngblood, *Optimization of Silica Silanization by 3-Aminopropyltriethoxysilane.* Langmuir, 2006. **22**(26): p. 11142-11147.

30.   Canton, G., et al., *Modified Stöber synthesis of highly luminescent dye-doped silica nanoparticles.* Journal of Nanoparticle Research, 2011: p. 1-8.

31.   Bae, J.A., et al., *Effect of pore structure of amine-functionalized mesoporous silica-supported rhodium catalysts on 1-octene hydroformylation.* Microporous and Mesoporous Materials, 2009. **123**(1-3): p. 289-297.

32.   Oldenburg, S.J., et al., *Nanoengineering of optical resonances.* Chemical Physics Letters, 1998. **288**(2-4): p. 243-247.

33.   Westcott, S.L., et al., *Formation and Adsorption of Clusters of Gold Nanoparticles onto Functionalized Silica Nanoparticle Surfaces.* Langmuir, 1998. **14**(19): p. 5396-5401.

34.   Kulkarni, S.A., S.B. Ogale, and K.P. Vijayamohanan, *Tuning the hydrophobic properties of silica particles by surface silanization using mixed self-assembled monolayers.* Journal of Colloid and Interface Science, 2008. **318**(2): p. 372-379.

35.   Decher, G., *Fuzzy Nanoassemblies: Toward Layered Polymeric Multicomposites.* Science, 1997. **277**(5330): p. 1232-1237.

36.   Manca, L. and et al., *In situ synthesis of Ag nanoparticles in polyelectrolyte multilayers.* Nanotechnology, 2007. **18**(32): p. 325601.

37.   Manca, L. and et al., *Controlled synthesis of pure and doped ZnS nanoparticles in weak polyion assemblies: growth characteristics and fluorescence properties.* Nanotechnology, 2009. **20**(27): p. 275601.

38.   Wang, L. and J. Sun, *Poly(allylamine hydrochloride)-dextran microgels functionalized with magnetic and luminescent nanoparticles.* Journal of Materials Chemistry, 2008. **18**(34): p. 4042-4049.

39.   Lutz, K., et al., *Biomimetic silica formation: Analysis of the phosphate-induced self-assembly of polyamines.* Physical Chemistry Chemical Physics, 2005. **7**(14): p. 2812-2815.

40.   Brunner, E., K. Lutz, and M. Sumper, *Biomimetic synthesis of silica nanospheres depends on the aggregation and phase separation of polyamines in aqueous solution.* Physical Chemistry Chemical Physics, 2004. **6**(4): p. 854-857.

41.   Sumper, M., S. Lorenz, and E. Brunner, *Biomimetic Control of Size in the Polyamine-Directed Formation of Silica Nanospheres.* Angewandte Chemie International Edition, 2003. **42**(42): p. 5192-5195.

42.   Rana, R.K., et al., *Nanoparticle Self-Assembly of Hierarchically Ordered Microcapsule Structures.* Advanced Materials, 2005. **17**(9): p. 1145-1150.

43.   Murthy, V.S., R.K. Rana, and M.S. Wong, *Nanoparticle-Assembled Capsule Synthesis: Formation of Colloidal Polyamine−Salt Intermediates.* The Journal of Physical Chemistry B, 2006. **110**(51): p. 25619-25627.

44.   Bagaria, H.G., S.B. Kadali, and M.S. Wong, *Shell Thickness Control of Nanoparticle/Polymer Assembled Microcapsules.* Chemistry of Materials, 2010. **23**(2): p. 301-308.

45.   Shea, K.J. and D.A. Loy, *Bridged Polysilsesquioxanes. Molecular-Engineered Hybrid Organic-Inorganic Materials.* Chemistry of Materials, 2001. **13**(10): p. 3306-3319.

46.   Luckarift, H.R., et al., *Enzyme immobilization in a biomimetic silica support.* Nat Biotech, 2004. **22**(2): p. 211-213.

47.   Caruso, R.A. and M. Antonietti, *Sol−Gel Nanocoating: An Approach to the Preparation of Structured Materials.* Chemistry of Materials, 2001. **13**(10): p. 3272-3282.

48.   Burns, A., H. Ow, and U. Wiesner, *Fluorescent core-shell silica nanoparticles: towards "Lab on a Particle" architectures for nanobiotechnology.* Chemical Society Reviews, 2006. **35**(11): p. 1028-1042.

49.   Arkhireeva, A., et al., *Synthesis of Organic-Inorganic Hybrid Particles by Sol-Gel Chemistry.* Journal of Sol-Gel Science and Technology, 2004. **31**(1): p. 31-36.

50.   Bauer, C.A., D.B. Robinson, and B.A. Simmons, *Silica Particle Formation in Confined Environments via Bioinspired Polyamine Catalysis at Near-Neutral pH.* Small, 2007. **3**(1): p. 58-62.

51.   Vrieling, E.G., et al., *Controlled Silica Synthesis Inspired by Diatom Silicon Biomineralization.* Journal of Nanoscience and Nanotechnology, 2005. **5**: p. 68-78.

52.   Baumann, F., et al., *On the Preparation of Organosilicon .mu.-Spheres: A Polycondensation in .mu.-Emulsion?* Macromolecules, 1994. **27**(21): p. 6102-6105.

53.   Tiarks, F., K. Landfester, and M. Antonietti, *Preparation of Polymeric Nanocapsules by Miniemulsion Polymerization.* Langmuir, 2001. **17**(3): p. 908-918.

54. Noda, I., T. Kamoto, and M. Yamada, *Size-Controlling Synthesis of Narrowly Distributed Particles of Methylsilsesquioxane Derivatives.* Chemistry of Materials, 2000. **12**(6): p. 1708-1714.

55. Delak, K.M. and N. Sahai, *Amine-Catalyzed Biomimetic Hydrolysis and Condensation of Organosilicate.* Chemistry of Materials, 2005. **17**(12): p. 3221-3227.

56. Patwardhan, S.V., N. Mukherjee, and S.J. Clarson, *Effect of process parameters on the polymer mediated synthesis of silica at neutral pH.* Silicon Chemistry, 2002. **1**(1): p. 47-54.

Chapter 2

Experimental Methods

2.1. Introduction

Synthesis of silica-hybrid nanoparticles is a two-steps method: formation of polymer salt aggregates (PSAs) followed by the addition of silicic acid. Figure 2-1 shows the scheme to form small or large silica hybrid nanoparticles by meticulously controlling the size of PSA. The following step of adding silicic acid solidifies the electrostatic-linking of the polymer and salt aggregates. In addition, some amine groups are exposed on the surface after the silicic acid hydrolyzes to the size of the PSA. The experimental details in formation of these cationic silica hybrid nanoparticles are presented below.
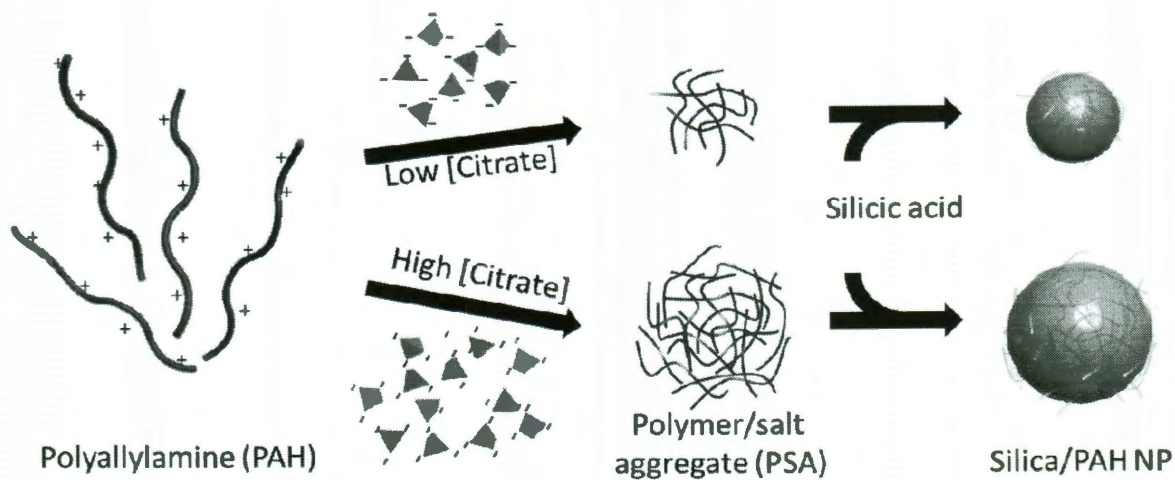
Figure 2-1. Synthesis schematic of silica/polymer nanoparticles (NPs) from polymer-salt aggregates (PSAs).

2.2. Chemical precursors

Polyallylamine hydrochloride (PAH, ~56 kDa, ~600 amines/chain), tetramethyl orthosilicate (TMOS, ≥99.9%), NaOH (≥ 98%), and Coomassie Brilliant Blue G dye (≥ 80%) were purchased from Sigma-Aldrich and used as-is. Trisodium citrate dihydrate salt (≥ 99%), NaCl (≥ 99%) and 1N HCl were sourced from Fisher Scientific. Materials used for the control samples are the following: silica mesoparticles (120 nm, concentration ~ 50 wt. %, Precision Colloids LLC), 3-aminopropyltriethoxysilane (APTES, ≥98%, Sigma-Aldrich), and ethanol (200 proof, Sigma-Aldrich). Deionized (DI) water from a Barnstead Nanopure Diamond System (18.2MΩ) was used for all experiments.

2.3. Polymer Salt Aggregates Synthesis

PSA synthesis is the most crucial step in determining the particle size of silica/polymer hybrid particles. PSAs using sodium tricitrate salt as a template for nanoparticles assembled capsules (NACs) synthesis were first reported by Rana et al.[1] Further improvement of this technique by the same group yielded nanosized aggregates.[2] To describe the concentrations of polymer (PAH) and salt (citrate) in the aggregate, a theoretical overall charge ratio is used for simplification:

$$R = \frac{[anion] \times [Z^-]}{[cation] \times [Z^+]}$$

where (PAH Z^+=600, citrate Z^-=3). With an R ratio set at 2, PAH concentrations were varied from 0.01 to 2 mg/mL to assess the average size and distribution of the PAH-citrate aggregates. These small-volume samples (#1-6, Table 2-1) were prepared by

adding PAH solution to a citrate solution in a 15-mL centrifuge tube followed by vortexing at speed '7' for 15 s (Fisher Scientific Mini Vortexer) with the concentration specified in Table 2-1. Using a PAH concentration of 0.1 mg/mL, citrate concentrations were varied from 143 to 200 μM to generate larger-volume samples (#7-11, Table 2-1). For these syntheses, the PAH solution was added to a citrate solution in a 100-mL beaker under constant magnetic stirring at 300 RPM for 2 min (Fisher Scientific Isotemp Hot Plate Stirrer), and the resulting suspension was left unstirred to age for 30 min. The larger volumes (10× more than those of samples #1-6) were needed to ensure sufficient sample amount for characterization.

Table 2-1. Parameters of samples prepared with #1-6 to test optimum PAH concentration for nano-scale aggregates growth. After finding the best PAH concentration, the citrate concentration was varied for sample #7-11.

Sample number	PAH concentration (mg/mL)	PAH solution volume (mL)	Citrate concentration (μM)	Citrate solution volume (mL)	Charge ratio R
1	0.01	1	3	2.5	2.00
2	0.05	1	14	2.5	2.00
3	0.10	1	29	2.5	2.00
4	0.50	1	143	2.5	2.00
5	1.00	1	286	2.5	2.00
6	2.00	1	571	2.5	2.00
7	0.10	10	143	25	1.00
8	0.10	10	157	25	1.10
9	0.10	10	171	25	1.20
10	0.10	10	186	25	1.30
11	0.10	10	200	25	1.40

2.4. Silica/polymer NP Synthesis

Silica/polymer NPs formed after adding silicic acid to a PSA suspension. An aqueous silicic acid solution (1 M) was prepared by combining TMOS with a dilute HCl solution (1 mM) and aging for a minimum of 20 min. The solution (pH = 3), which was not used after 24 hr when it turned cloudy, contains monosilicic acid $Si(OH)_4$ and dimers, trimers, and larger oligomers of monosilicic acid. These species favor the formation of siloxane bonds (Si-O-Si) and minimization of the silanol groups (Si-OH), which led to the formation of 2-3 nm particles at the end of aging period [3, 4]. The silicic acid solution (10 mL) was added to a 30-min-old PSA suspension (35 mL, sample #7-11 in Table 2-1) in a 100-mL flask followed by stirring at 300 rpm for 2 min and aging for 2.5 hr. The resulting suspension was washed by centrifuging at 22,500 relative centrifugal force for 30 min to remove any excess silicic acid, dispersing into DI water, and repeating once more. The particles are referred hereafter as "silica/PAH" or "hybrid" NPs.

2.5. Control Sample Synthesis

Silica/PAH NPs were compared against bare SiO_2 and SiO_2 modified with amine surface groups. For the preparation of "APTES-SiO_2," a suspension of SiO_2 mesoparticles (2 mL) was diluted into DI water (80 mL) and centrifuged at 3,500 RCF for 30 min. The resulting precipitate was dispersed into ethanol and centrifuged; this cleaning step was performed twice. Then APTES (500 µL) was added to a vigorously stirring SiO_2 mesoparticles suspension, for a final APTES concentration of 26.5 mM.

The solution was left stirring overnight, and centrifuged and dispersed into ethanol (20mL) for storage. The final suspension had a pH of 8.1, SiO_2 concentration of 5 wt %, and particle concentration of 2.15 x 10^{14} #/mL). For zeta potential testing, 50 μL was added to 3 mL DI water.

2.6. Characterization

Polymer salts aggregates and silica hybrid nanoparticles were characterized by several techniques: dynamic light scattering, zeta potential measurements, thermal gravimetric analysis, UV-Vis spectrophotometry, scanning electron microscopy, and transmission electron microscopy. The processes of each technique are described below with emphasis on dynamic light scattering and zeta potential because DLS provides quick size analysis before further silicification steps are taken. Zeta potential provides the potential measurement in which the surface charge density can be calculated from. For other techniques, a brief discussion and methodology to prepare the sample for measurements are given.

2.6.1 Dynamic Light Scattering

Dynamic light scattering was used to quickly screen polymer-salt aggregates size distribution profile and average size before the addition of silicic acid. All particles or molecules in suspension experienced Brownian motion due to their thermal energy, $k_B T$ (k_B being the Boltzmann constant, T = temperature). If the particles or molecules were irradiated with a laser, the intensity of the Rayleigh scattering would vary according to the size of the product in question. The smaller particles would experience more

movements compared to larger one. [5] The intensity fluctuation recorded yields the velocity of the Brownian motion and hence the particle size.

Analysis of the signal is the key to dynamic light scattering where the diffusion coefficient and subsequently the hydrodynamic diameter. The signals recorded are quite random and would yield minimal information as is. However, when the signals are being examined and compared at different instances of time, information regarding the system can be extracted. This comparison is called the autocorrelation function (ACF). For a general analysis of a monodisperse distribution system, the resulting ACF would be an exponential decay function

$$|g^1(\tau)| = exp(-\Gamma\tau)$$

with Γ being the decay rate. For a polydisperse system, the analysis would be more complicated because the whole system would have to be treated as a summation of monodisperse suspensions. The decay rate is related to the translational diffusion coefficient (D) as follows

$$D = \frac{\Gamma\lambda^2}{\left(4n_0\pi \ sin\frac{\theta}{2}\right)^2}$$

with n_0 being the refractive index of the solution, θ is the scattering angle (90 degrees for our instrument setup), and λ is the laser wavelength (656 nm). If the laser wavelength is changed to other frequency, the ACF and the decay rate, Γ, will differ resulting in the same diffusion coefficient. From the translational diffusion coefficient, the hydrodynamic diameter (R_h) can be calculated using the Stokes-Einstein relation

$$R_h = \frac{k_B T}{6\pi\eta D}$$

where k_B is the Boltzmann constant, T the operating temperature, and η is the solution viscosity.[6]

The Brookhaven Instrument DLS used for this measurement has built-in algorithms to calculate the size from the autocorrelation function specifically CONTIN and NNLS. Additionally, the particles in suspension can also be weighted based on intensity or number. Intensity-based weighs the particle on the amount of scattering a particle or molecule produces, which also means that larger particles will scatter more compared to smaller particles. This weighing method produces an average size that is geared more toward the larger size particles. Number weighted average size takes the intensity-based NNLS or CONTIN results and apply log-normal function to account for smaller particle intensity; which is equal to larger particles.[7] In addition, previous studies on silica colloids compared SEM average sizes to DLS average size (NNLS intensity based, NNLS number based, CONTIN intensity based, and CONTIN number based) and it was found that CONTIN number based average size comes within 1% of the SEM average size.[6] All DLS values used within this study are number-based CONTIN analyses.

2.6.2 Zeta Potential

The average surface charges of silica/PAH NPs, bare SiO_2, and amine-modified SiO_2 were analyzed through zeta potential measurements with the same ZetaPALS instrument equipped with a dip-in electrode. A particle suspension (25 μL) was added to

a NaCl solution (1.48 mL, 10mM) in a cuvette. The electrophoretic mobility (μ_e) of each sample was measured 10 times (with 20 cycles per measurement) at 25°C. Zeta potential values (ζ) were derived from the electrophoretic mobility of each sample with the relation

$$\zeta = \mu_e \eta / \varepsilon_r \varepsilon_0 \, ,$$

where η is the viscosity of the medium, ε_r is the dielectric constant of the medium, and ε_0 is the permittivity of free space. The stability of a NPs suspension can be determined by the values in Figure 2-2. [8]
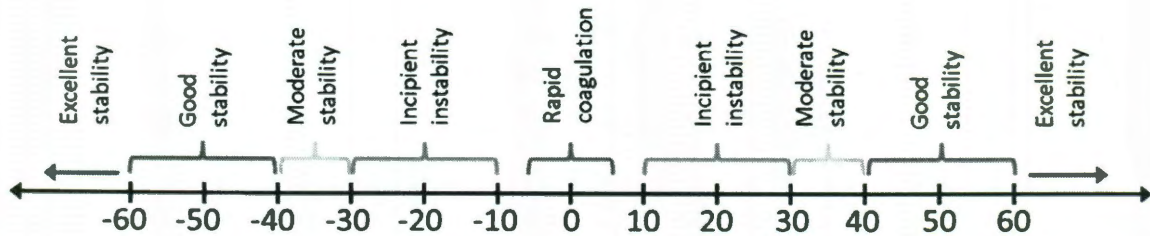
Figure 2-2. Stability of colloids in suspension based of zeta potential value.

The stability of particles in suspension can be described by the Derjaguin, Verwey, Landau, and Overbeek theory (DLVO theory), which suggests that the stability is based on the total potential within the system. At low zeta potential 30 mV$\leq \zeta \leq$ 30 mV, there are not enough force between particles to prevent flocculation or coagulation.[8] The most important factor that affects the zeta potential is the pH of the solution. If more alkali is added to the suspension of particles, resulting in an increased pH, more negative charge will be attracted to the particles and vice versa for acid. Due to this pH effect, the zeta potential of particles suspension tends to be positive at acidic pH and negative at basic pH. The point where the magnitude of zeta potential is zero is

called the isoelectric point. At the isoelectric point, the suspension of the particle is the least stable, which results in flocculation.

Zeta potentials are measurements at the slipping plane of the double layer for a charged particle in solution. As in Figure 2-3, a charged particle is surrounded by liquid that can be characterized as two layers. The first layer of ionic charged liquid consists of highly attracted counterions, this is also known as the Stern layer.[9] Further away from the Stern layer of the charged particle is a freely bound ions/fluid layer that depends on the applied electric potential.
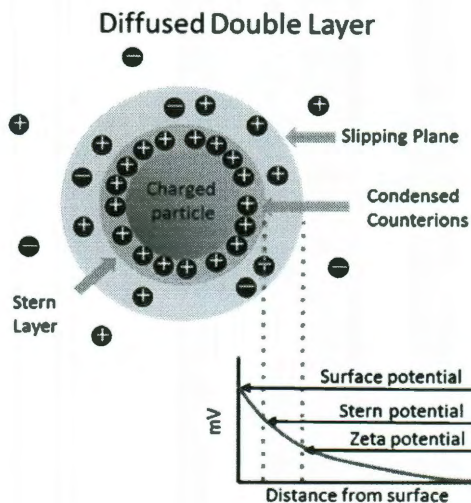
Figure 2-3. The diffuse double layer of a charged particle and its corresponding surface charge base on distance from surface. Highly bound counter ions exist within the Stern Layer. Zeta potential values are measured at the slipping plane, not the actual surface potential.

This layer of freely moving ions is the diffuse layer with zeta potential measurement at the edge of the diffuse layer, which is the slipping plane. The ions within these two layers will move with the particle as the particle moves, ions outside this region

will not move with the particle.[10] The potential (ψ) from the particle center can be described by the Debye-Huckel approximation

$$\psi(r) = \psi_d \frac{a}{r} exp(-\kappa(r - a))$$

where ψ_d is the potential at the Stern layer, a is the particle radius, and κ^{-1} is the Debye length.[11] By knowing the Stern potential, the capacity of the surface charge (C) can be calculated by

$$C = \frac{\sigma}{\psi_0 - \psi_d}$$

with σ as the surface charge density and ψ_0 as the charge at the particle surface. For silica surfaces, the capacity is consistent at 2.9 F/m^2 regardless of electrolyte concentration or surface geometry. With two unknowns, ψ_0 and ψ_d, the surface charge density cannot be determined. However, the surface charge density can be related to the Stern potential by the Grahame equation (for a flat surface)

$$\sigma(\psi_d) = \frac{2\varepsilon_r\varepsilon_0\kappa}{\beta e} \sinh\frac{\beta e\psi_d}{2}$$

where κ^{-1} is the Debye length defined as $\kappa^2 = 0.304/(I)^{0.5}$, I is the electrolyte concentration (for this study, the electrolyte concentration is kept at 10mM NaCl), β is the thermal energy k_BT, k_B is the Boltzmann constant, T is the temperature, and e is the charge of an electron. With a curved surface geometry taken into account, the modified equation is

$$\sigma(\psi_d) = \frac{2\varepsilon_r\varepsilon_0\kappa}{\beta e}\sinh\frac{\beta e\psi_d}{2} + \frac{2}{\kappa a}\tanh\frac{\beta e\psi_d}{4}$$

where a is the radius of the charged particle. This equation can calculate the surface potential value within 5% of the actual value when $\kappa a \geq 0.5$.[12] For this study calculation, one assumption for calculating the surface potential is making zeta potential equal to the Stern potential. This assumption will report a lower surface charge density because $\zeta < \psi_d$; however, it is a good approximation of the magnitude of the surface charge.

2.6.3 Thermal Gravimetric Analysis

TGA is utilized to determine thermal stability of polymer-salt aggregates compared with silica-hybrid, control silica, and functionalized silica nanoparticles. The NPs were dried from suspension in a vacuum oven at 80°C for 24 hr, of which approximately 50 mg were loaded into an alumina crucible. The sample was heated to 800 °C at a ramp rate of 2°C/min under flowing argon gas.

The measurements reported highly precise weight change in relation to change in temperature. The weight change can either increase or decrease through different processes. Weight increase can happen through absorption or oxidation with a reactive atmosphere. Decomposition of chemical bonds, evaporation of volatiles, or desorption are the processes that result in weight loss.[13] However, the argon atmosphere that is employed in these measurements reduces any possibility of absorption or oxidation processes. The weight loss seen in polymer-salt aggregates, silica hybrid, control silica, and functionalized silica were due to either decomposition, evaporation and/or desorption processes.[14]

2.6.4 UV-vis Spectroscopy

UV-vis spectroscopy is a measure of light absorbance or transmittance. This measurement is used for the Coomassie Brilliant Blue G (CBBG) dye study in the presence of silica particles suspension with different surface charges. For the Coomassie blue tests, silica/PAH NPs were centrifuged (22,500 RCF, 30 minutes), washed with 50 mL DI water, and repeated three times. These were then dispersed in 2.75 mL water. The comparison samples were prepared by adding SiO_2 mesoparticles (50 μL) to DI water (2.7 mL), and adding APTES-SiO_2 mesoparticles (50 μL) to DI water (2.7 mL). To each of these three suspensions, an HCl solution (150 μL, 1 M) and a Coomassie Brilliant Blue G solution (100 μL, 1.2 mg/mL) were added. Each sample (3 mL) was analyzed through UV-vis spectroscopy on a Shimadzu UV-2401PC Spectrophotometer using 1-cm path length polystyrene cuvettes. Scans were performed from 300 nm to 900 nm at 1-nm wavelength intervals.

The instrument used for these measurements is based on a double beam design. This design is an improvement over the single beam design where the sample has to be measured twice: once with the sample and second without the sample, which would be used as an intensity reference. The double beam design consolidates two measurements into one by splitting the light source into two as in Figure 2-4. This design allows instant calculation of absorbance and transmittance by comparing the light intensity of a reference sample with the actual sample.[15] From measuring each sample, the peak absorbance varies according to the surface charge of the particles in suspension with

CBBG. Further explanation in section IV will explain the significance of absorbance peak of CBBG in silica suspension with different surface charges.
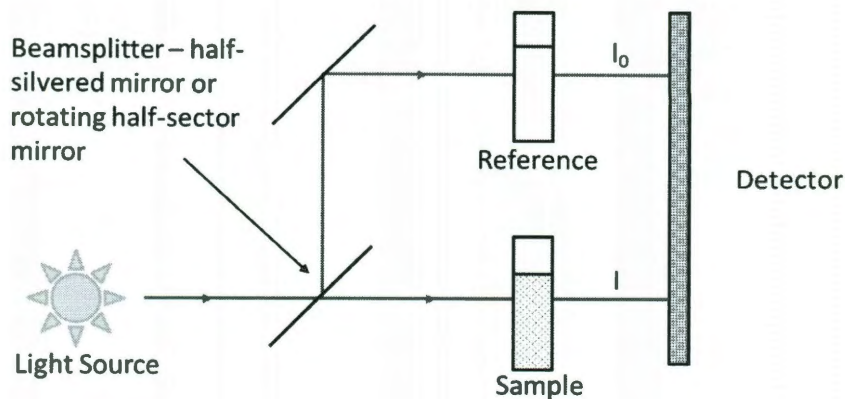
Figure 2-4. Schematic of a typical double beam UV-vis spectrophotometer.

2.6.5 Scanning and Transmission Electron Microscopy

Scanning electron microscopy (SEM) was performed on the silica/polymer NPs using a FEI Quanta 400 operating at 15kV. A NP suspension sample was subjected to ultracentrifugation at 100,000 RCF for 1 hr, and the collected material was placed onto a carbon tape-covered aluminum sample stub, and left overnight to dry at room temperature. The sample was sputter coated with gold to minimize charging artifact with non-conducting samples. The mean and median sizes, and standard deviation values were estimated for each sample using ImageJ analysis of 1000 particles in the SEM images. The scheme for a typical SEM instrument is shown in Figure 2-5. The images obtained from SEM are based on back scattered electrons.
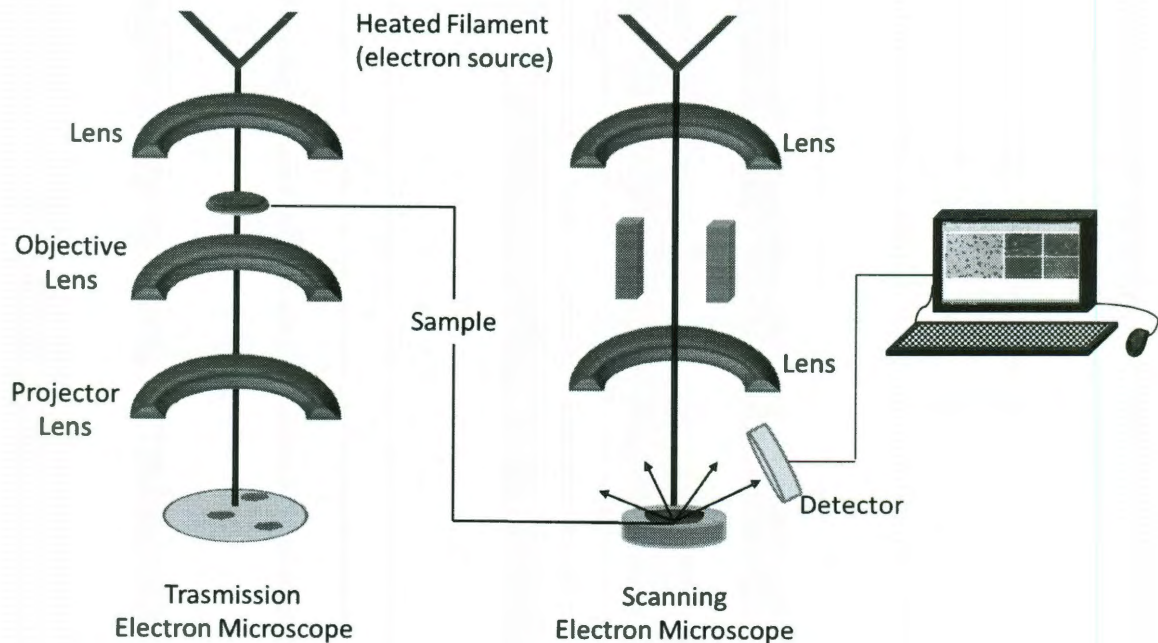
Figure 2-5. Scheme of transmission and scanning electron microcope. SEM is based on scattered electrons while TEM is based on transmitted electrons through the sample.

Transmission electron microscopy (TEM) was used mostly to determine the solidity of silica/PAH particles. TEM is based on transmission of electrons through a sample. The difference in gray level is due to the electron density of the viewing sample: denser electron density such as gold or silver will appear darker than silica. Sample preparation for TEM included loading the sample (10 µL) onto a Holey copper grid purchased from Ted Pella and left over night to dry. The sample was loaded into a JEOL 1230 High Contrast Transmission Electron Microscope and set to 80kV.

2.7. References

1. Rana, R.K., et al., *Nanoparticle Self-Assembly of Hierarchically Ordered Microcapsule Structures.* Advanced Materials, 2005. **17**(9): p. 1145-1150.
2. Murthy, V.S., R.K. Rana, and M.S. Wong, *Nanoparticle-Assembled Capsule Synthesis: Formation of Colloidal Polyamine–Salt Intermediates.* The Journal of Physical Chemistry B, 2006. **110**(51): p. 25619-25627.
3. Bauerlein, E., *Biomineralization: progress in biology, molecular biology and application.* 2nd ed. 2004: Wiley-VCH.
4. Iler, R.K., *The Chemistry of Silica.* 1979: John Wiley & Sons, Inc.
5. B. J. Berne, R.P., *Dynamic Light Scattering.* 2000, Mineola, NY: Dover Publications Inc.
6. L. H. Hanus, H.J.P., ed. *Characterizing Colloidal Materials using Dynamic Light Scattering.* Surface Characterization Methods: Principles, Techniques, and Applications, ed. A.J. Milling. 1999, Marcel Dekker: New York, NY. 199-248.
7. Thomas, J.C., J. Colloid Interface Sci., 1987. **117**(1): p. 187-192.
8. Materials, A.S.f.T.a., *"Zeta Potential of Colloids in Water and Waste Water.* 1985.
9. Russel, W.B., D.A. Saville, and W.R. Schowalter, *Colloidal Dispersions, Cambridge Monographs on Mechanics and Applied Mathematics.* 1989, Cambridge: Cambridge University Press.
10. Instruments, M., *Zeta Potential - An Introduction in 30 Minutes*, in *Zetasizer Nano Series*.
11. Debye, P. and E. Hückel, *The theory of electrolytes. I. Lowering of freezing point and related phenomena.* Physikalische Zeitschrift 1923. **24**: p. 185-206.
12. Behrens, S.H. and D.G. Grier, *The charge of glass and silica surfaces.* The Journal of Chemical Physics, 2001. **115**(14): p. 6716-6721.
13. S. N. Bhattacharya, R.K.G., M. R. Kamal, *Polymeric Nanocomposites Theory and Practice.* 2008, Munich, DE: Hanser Verlag.
14. Mueller, R., et al., *OH Surface Density of SiO2 and TiO2 by Thermogravimetric Analysis.* Langmuir, 2002. **19**(1): p. 160-165.
15. Kyte, J., *Structure in protein chemistry.* 2007: Garland Science.

Chapter 3

Analysis of Silica/polymer Particles

3.1. Introduction

This chapter discusses the results of polymer-salt aggregate (PSA) formation by varying the PAH and citrate concentration. After determining the optimum concentration, a bulk amount (10 times volume, 35mL total) at a predetermined range was synthesized followed by silicic acid treatment. The resulting silica/PAH or silica/hybrid nanoparticles' diameter and monodispersity was then analyzed with SEM images. The thermal stability of the hybrid nanoparticles were found to have similar characteristic as pure silica and functionalized silica.

3.2. Optimization of Polymer-Salt Aggregate Synthesis

The effect of PAH concentration on the PAH-citrate aggregate size was studied towards the synthesis of sub-100 nm silica/polymer particles. PAH concentrations were systematically varied while the charge ratio was set at R = 2 (samples #1-6, Table 3-1). All samples turned cloudy as soon as the PAH and citrate solutions were combined. Samples #1-3, which corresponded to low PAH concentrations (0.01, 0.05, 0.1 mg/mL), contained smaller PSA's showing little growth over time, whereas samples #4-6, which corresponded to high PAH concentrations (0.5, 1, 2 mg/mL), contained much larger particles and grew over the course of 30 min, similar to previous observations [1] (Fig. 3-1).
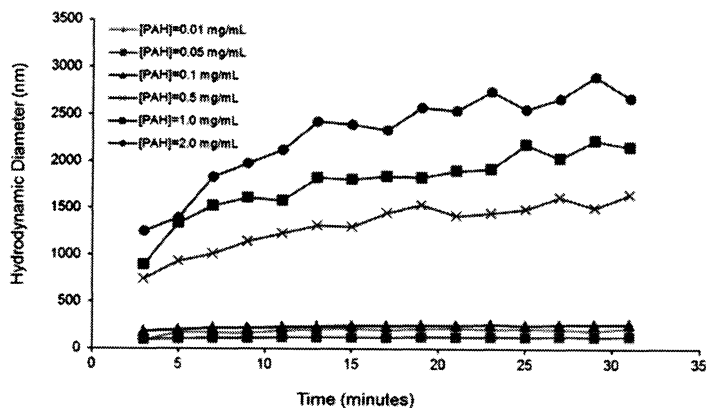
Figure 3-1. Hydrodynamic diameter of polymer-salt aggregates with different concentrations of PAH with R ratio = 2.

In fact, the PAH-citrate aggregates prepared at high PAH concentrations increased by >900 nm (Table 3-1). At low PAH concentrations, the maximum increase in the hydrodynamic diameter (D_h) was less than 100 nm. For subsequent studies, the PAH concentration of 0.1 mg/mL was chosen as the optimum value for minimal aggregate growth and for formation of a sufficient amount of aggregates.

Table 3-1. Samples' number-weighted hydrodynamic diameters and their growth over 30 min. The amount of PAH and citrate are specified in Chapter 2.3.

Sample	D_h at 3 min (nm)	D_h at 30 min (nm)	Growth rate (nm/min)
1	87	220	4.93
2	100	134	1.26
3	187	266	3.93
4	747	1654	33.59
5	834	2173	49.59
6	1029	2696	61.74
7	30	36	0.22
8	37	48	0.41
9	57	68	0.41
10	66	84	0.67
11	88	111	0.85

The effect of charge ratio R on the PAH-citrate aggregate size was studied next, with the PAH concentration set at 0.1 mg/mL. The narrow R range of 1.0-1.4 was studied (samples #7-11, Table 3-1), as slow aggregate formation occured around these values [1] At the low value of R = 1.0, the PSA size was 30 nm at 3 min, growing to 36 nm at 30 min (growth rate ~ 0.22 nm/min). At the high value of R = 1.4, the PSA size was 88 nm at 3 min, growing to 111 nm at 30 min (growth rate ~ 0.85 nm/min). R values less than 1.0 were expected to yield PAH-cirate aggregates smaller than 30 nm. In fact, R = 0.9 yielded PSA sizes of ~20 nm. However, the size distribution measurements were difficult to reproduce due to the low scattering intensity of the suspension. Thus, R values smaller than 1.0 were not studied further.

The intermediate R values resulted in PSA sizes and growth rates that were between those at R = 1.0 and 1.4 at all times (Fig. 3-2a). The PSA's grew between 20% and 30% for all R values tested. Macroscopically, the PAH-citrate suspensions did not turn cloudy when the PAH and citrate solutions were combined, and they remained clear for at least 2 hr after synthesis.
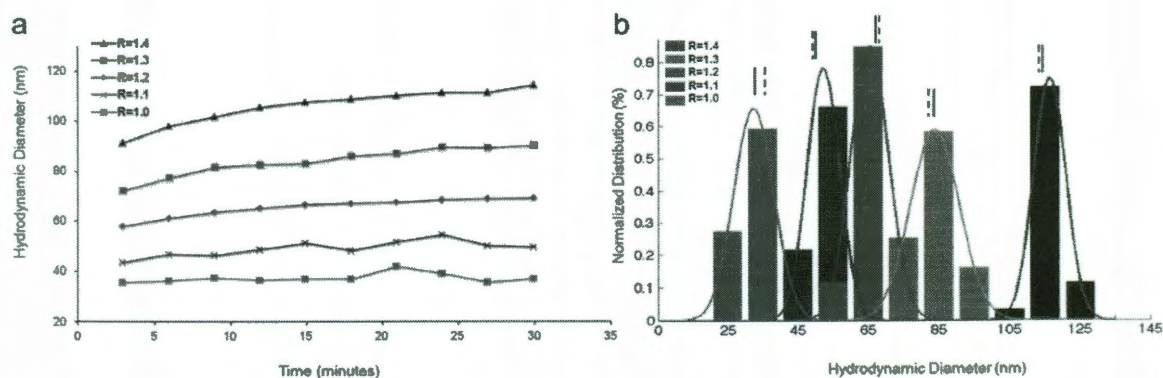
Figure 3-2. (a) Number-average hydrodynamic diameters of PAH-citrate colloidal aggregates (R range of 1.0 and 1.4) monitored over a period of 30 min. (b) Size

distributions measured at t = 30 min, shown with Gaussian distributions and mean (solid line) and median (dashed line) values marked.

The size distributions of the PAH-citrate aggregates prepared at the different R values were analyzed at 30 min (Fig. 3-2b, Table 3-2). The number-weighted mean sizes for each sample were close, but not equal, to the number-weighted median sizes (*i.e.*, D_h of the most populous bin size). Assuming a Gaussian fit, the standard deviation for each R value was in the 6-10 nm range, giving relative standard deviations (RSD's) in the 6 to 22% range. With "monodisperse," "narrow," and "broad" distributions having RSD's of 5%, 5-10%, and >10% [2, 3], the PSA's formed at R = 1.4 were narrow in size and PSA's formed at the other R values were broad in size.

Table 3-2. DLS hydrodynamic diameter measurements of PAH/citrate aggregates showed relationship between diameter and charge ratio R. In addition, the standard deviation (σ), RSD, and median D_h are shown.

Charge ratio R	Polymer Salt Aggregates			
	mean (nm)	σ (nm)	RSD (%)	median (nm)
1.0	36	8.0	22	38
1.1	48	6.5	14	47
1.2	68	7.5	11	69
1.3	84	9.7	12	83
1.4	111	6.4	6	111

3.3. Silica/polymer Nanoparticle Formation

Silicic acid was added to PSA suspensions of different R ratios to form the silica/polymer hybrid particles. We previously showed that silicic acid addition to meso-sized and

micron-sized PSA's led to the formation of solid silica/polymer particles [4]. The diffusion/deposition model used to understand microparticle formation was based on the idea that silicic acid (as silicate oligomers and 2-3-nm particles) diffuses and deposits throughout the PSA interior, whereas larger, ~10-nm silica NPs diffuse through only the outer corona of the PSA before they deposit to form thick-shelled hollow microspheres [5]. Silicic acid is a metastable suspension of reactive silicate species, and so its deposition within the PSA interior is likely followed by polymerization of the silicate species via condensation reaction. The PSA interior contains a high content of amine groups of the PAH polymer, suggesting that formation of these silica/polymer hybrid particles is akin to biosilicification processes that generate naturally occurring diatoms [6-10].

To verify that silicic acid reacted with the PSA's, we compared their ionic strength stability to that of the PSA suspensions by suspending the hybrid particles and PSA's in a high-salinity solution and measuring their hydrodynamic diameters. As a representative sample, a PAH/citrate aggregate suspension prepared at R = 1.4 had a mean D_h average of 111±6.4 nm (Table 3-2). When the suspension ionic strength was raised to 1 M with NaCl, aggregates were no longer detectible via DLS and no D_h size was recorded, consistent with our previous observation that high salinity causes the PSA's to dis-assemble [5]. After addition of silicic acid, the PAH/citrate aggregate suspension had a number-weighted mean average of 139±25 nm (Table 3-3). This PAH/citrate/silicic acid mixture was added to a 1 M NaCl solution; DLS analysis did not change the number-weighted mean average, indicating that silicic acid reacted with the PSA's to

form salt-tolerant particles. These particles could be centrifuged and re-dispersed into water, and could be imaged under ultrahigh vacuum conditions (Fig. 3-3).

Table 3-3. SiO$_2$/PAH hybrid particle size information from DLS and SEM analysis.

Charge ratio R	DLS of particles in wet state				SEM of particles in dried state			
	mean (nm)	σ (nm)	RSD (%)	median (nm)	mean (nm)	σ (nm)	RSD (%)	Median (nm)
1.0	38	3	9	38	42	9	21	42
1.1	52	5	10	52	49	7	14	47
1.2	76	7	9	76	73	13	18	72
1.3	104	12	11	107	95	15	16	97
1.4	139	25	18	134	106	18	17	112
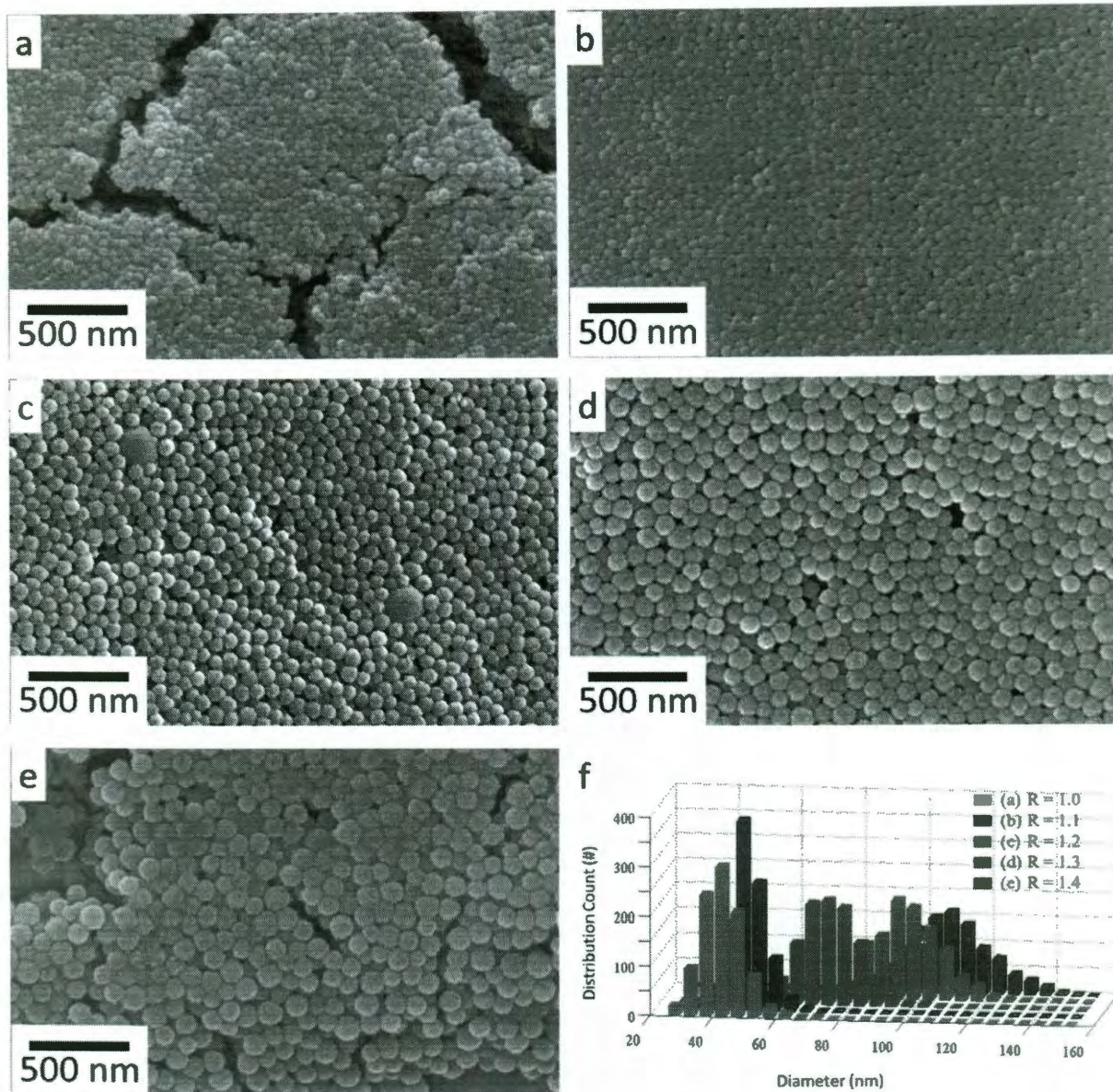
Figure 3-3. SEM images at 100,000× magnification of SiO_2/PAH particles formed from PAH/citrate aggregates prepared with R = (a) 1.0, (b) 1.1, (c) 1.2, (d) 1.3, and (e) 1.4. (f) Size histograms of SiO_2/PAH particles. ~1000 particles were analyzed per sample.

DLS analysis indicated SiO_2/PAH particles prepared at all the different charge ratios had unimodal size distributions. The distributions were narrow for R = 1.0, 1,1, and 1.2, and broad for R = 1.3 and 1.4. The mean average D_h values were consistently larger

than the corresponding D_h values of the parent PAH/citrate aggregates (Table 3-3). At smaller charge ratios, silicic acid addition led to minimal increase in size.

SEM analysis of dried SiO_2/PAH particles corroborated the increase in DLS-detected particle size with charge ratio, with the particles having broad size distributions (RSD ~ 14-21%) (Fig. 3-3f). All charge ratios that were studied yielded silica/polymer hybrid NPs, with R = 1.4 giving particles that were close to the nanoparticle/mesoparticle demarcation. The SiO_2/PAH particles were solid and not hollow (Fig. 3-4), consistent with silicic acid diffusing and depositing throughout the PSA interior and in accordance with the diffusion-deposition model [5].
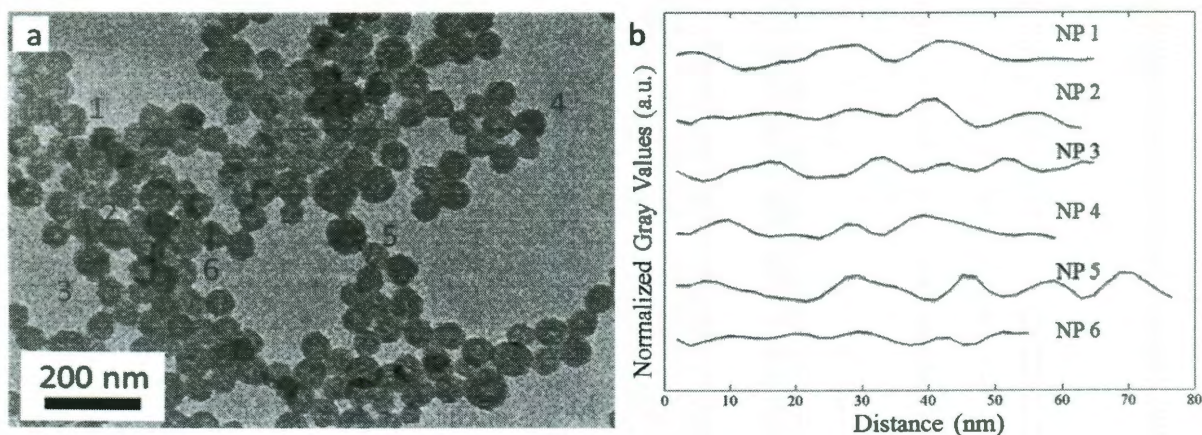
Figure 3-4. a) TEM image of silica/hybrid at R=1.4. b) Six randomly picked particles were analyzed to have consistent grayness based on the line-profile for each particle done in ImageJ, which signified that there were materials across the diameter. The inconsistent gray values suggest that these particles are porous and not hollow.

3.4. Organics Content of Silica-Hybrid Particle

TGA was employed to assess the organic content of SiO_2/PAH NPs prepared at R = 1.0 and 1.4 (Fig. 3-5). SiO_2/PAH NPs prepared at R = 1.0 lost ~21 wt% at a

temperature of 150 °C, due to residual water entrained within the hybrid particles, suggesting the presence of internal porosity. An additional 5 wt% from 150-800 °C, indicating that the dried hybrid NPs prepared at R = 1.0 content had an organics content of ~6.3 wt%. If the organics content were assumed to be entirely PAH, then each 42-nm hybrid particle is calculated to contain ~40 PAH chains. Hybrid particles prepared at R = 1.4 lost ~14 wt% at a temperature of 150 °C and ~11 wt% between 150 °C and 800 °C. The organic content of these 106-nm particles (~13%, equivalent to ~1700 PAH per particle) was double that of the 42-nm particles, suggesting that particles prepared at intermediate charge ratios have intermediate organics content also.
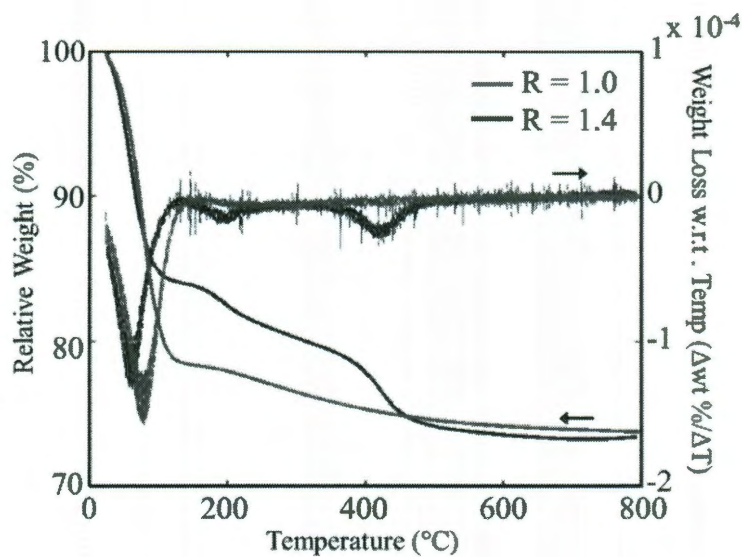
Figure 3-5. TGA profile of SiO_2/PAH hybrid NPs at R = 1.0 and 1.4.

3.5 Analysis of SiO$_2$/PAH NP Surface Charge

Coomassie brilliant blue (CBB) is used in protein assays [11, 12] and protein gel staining protocols [13], due to its ability to bind electrostatically to the positively charged ammonium groups of proteins and its colorimetric response after binding. CBB can be used to characterize amine groups on particle surfaces, though quantification is difficult to perform accurately [14]. The dye molecule (with pK$_a$ values of 1.15 and 1.82 [15]) exists as predominantly cationic, neutral, and anionic species in the pH ranges of <0.39, ~1.3, and >1.3, respectively; these species correspond to UV-vis absorbance peaks of 470 nm, 650 nm, and 590 nm, respectively [11, 12]. The anionic and neutral form of CBB can be seen at pH values of 1.3 and 6.0, agreeing with the reported peak absorbance (Fig. 3-6 a,b). At pH 1.6, a water solution of CBB had an absorbance peak of ~607 nm, indicating the presence of both the CBB anionic and neutral form (Fig. 3-6c). The red-shifting of the absorbance peaks with increasing solution acidity reflects a larger proportion of neutrally charged CBB versus the anionic form.
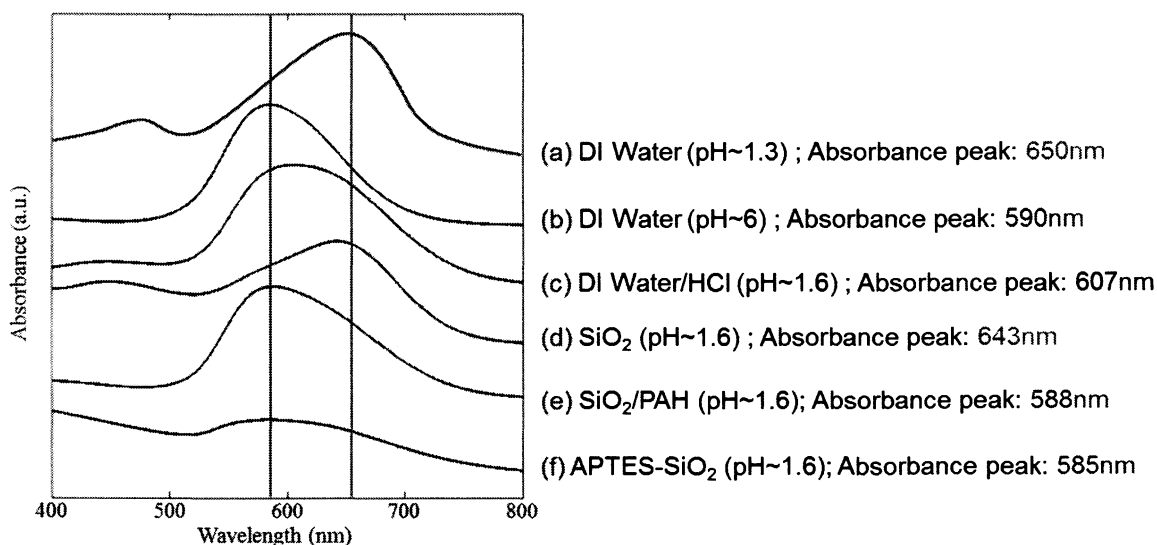
Figure 3-6. UV-vis spectra of CBB in (a) DI H$_2$O (pH ~ 1.3), (b) DI H$_2$O (pH ~ 6), (c) H$_2$O/HCl (pH ~ 1.6) only, and H$_2$O/HCl suspensions (pH ~ 1.6) of (d) bare SiO$_2$, (e) hybrid NPs, and (f) APTES-SiO$_2$.

An acidified CBB solution containing bare SiO$_2$ particles had a red-shifted absorbance peak at 643 nm, indicating that the silica essentially converted the CBB anion to its neutral form at pH 1.6. Point of zero-charge (pzc) values for SiO$_2$ are typically reported as ~2 [7, 16], suggesting the bare SiO$_2$ particle surface gained a net positive charge at pH 1.6 and neutralized the CBB via electrostatic binding. An acidified CBB solution containing SiO$_2$/PAH hybrid and APTES-SiO$_2$ particles had absorbance peaks at ~585 nm blue-shifted from 607 nm, indicating the population of anionic CBB was increased in the presence of the particles. This color shift can be attributed to the particle surfaces being positively charged, which electrostatically stabilized the otherwise anionic CBB form into its neutral form [15]. Importantly, the CBB colorimetric test indicated the SiO$_2$/PAH hybrid particles carried a positive surface charge, which can only come from the PAH amine groups being exposed at the particle surface.

Zeta potential measurements were made for the three silica particle types in the pH range of 2.5-11.5, to determine pzc and surface charge density values (Figure 3-7). Bare SiO_2 particles were negatively charged in the entire pH range, consistent with SiO_2 having an pzc of ~2 [7, 16]. APTES-SiO_2 particles, in comparison, were negatively charged above pH 10 and positively charged below pH 10. The pzc of APTES-SiO_2 was therefore ~10, close to the pK_a of the propylamine surface groups (pK_a ~ 10.6 [17]). SiO_2/PAH hybrid NPs (prepared at R=1.0) had an effective pzc of ~5, lower than the pK_a value of PAH (8.5 [18]), indicative of negatively charged silica portion at the hybrid NP surface.
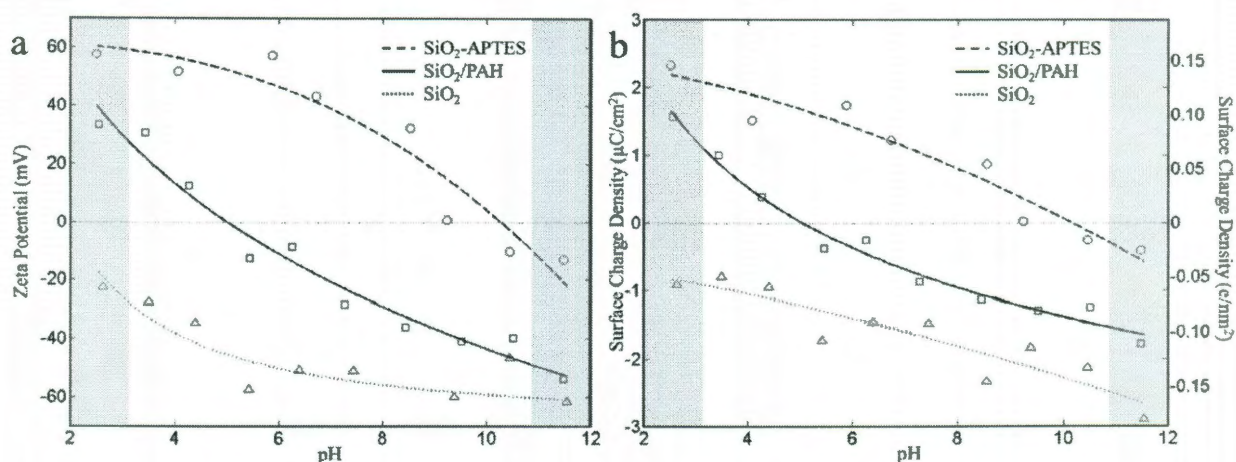
Figure 3-7. (a) Zeta potential and (b) calculated surface charge density values of SiO_2/PAH, bare SiO_2, and APTES-SiO_2 particles at different pH values. The gray-colored portions of the graphs indicate the ionic strength being higher than 10 mM, which was taken into account when calculating surface charge density.

The surface charge density values for the three silica particle types were calculated in the pH range of 2.5-11.5 from the zeta potential measurements (Figure 3-7b). At any pH value, the hybrid particles had zeta potential and surface charge values

between those of the bare and aminated SiO_2 particles. The SiO_2/PAH and APTES-SiO_2 particles had comparable charge densities (~1 $\mu C/cm^2$) at pH values of ~3.5 and ~8, respectively. Curiously, SiO_2/PAH and bare SiO_2 particles had comparable charge densities (~-1 $\mu C/cm^2$) at pH values of ~8 and ~3, respectively.

Surface charge density values at pH 4, 7, and 10 were calculated by interpolating from the collected data (Table 3-4). At pH 7, the values for bare SiO_2, SiO_2/PAH NPs, APTES-SiO_2 were -1.48, -0.57, and +1.22 $\mu C/cm^2$, respectively. In terms, of effective charge per nm^2, these values correspond to -0.093, -0.036, and +0.076 $\#/nm^2$, respectively. These values reflect the presence of silica surface hydroxyl groups, and for the amine-containing particles, the presence of surface amine groups. Maximum coverage of a silica surface by APTES was reported to be 1.52 $\#/nm^2$ [19], indicating the amine surface densities of SiO_2/PAH NPs (as well as APTES-SiO_2) were well below maximum coverage. The low values can be attributed to the use of zeta potential values to approximate the actual surface potential values of particles.

Table 3-4. Zeta potential and surface charge density values of bare SiO_2, SiO_2/PAH hybrid, and APTES-SiO_2 interpolated at three different pH values using the best-fit curves. I = 10 mM.

pH	Bare SiO_2			SiO_2/PAH hybrid			APTES-SiO_2		
	ζ (mV)	σ ($\mu C/cm^2$)	($\#/nm^2$)	ζ (mV)	σ ($\mu C/cm^2$)	($\#/nm^2$)	ζ (mV)	σ ($\mu C/cm^2$)	($\#/nm^2$)
4	-35	-0.89	-0.056	+18	+0.55	+0.034	+51	+1.51	+0.094
7	-51	-1.48	-0.093	-19	-0.57	-0.036	+43	+1.22	+0.076
10	-63	-1.99	-0.125	-39	-1.25	-0.078	-10	-0.27	-0.017

The protonated amine surface density for the hybrid and APTES-SiO$_2$ particles can be estimated from the values in Table 3-4. The $\sigma_{measured}$ (= $\sigma_{protonated-amine}$ + $\sigma_{SiO2-hydroxyl}$) can be considered the net sum of positive surface charge from the PAH amine portion of the surface ($\sigma_{protonated-amine}$) and negative surface charge from the silica hydroxyl portion ($\sigma_{SiO2-hydroxyl}$ measured for bare SiO$_2$). For hybrid particles at pH 4 then, the protonated amine surface density was +0.09 #/nm^2 ($\sigma_{protonated-amine}$ = $\sigma_{measured}$ - $\sigma_{SiO2-hydroxyl}$ = +0.034 - -0.056). The values at pH 7 and 10 were +0.057 and +0.047 #/nm^2, respectively, consistent with the amine portion of the surface became less positive with higher pH values. For APTES-SiO$_2$ particles, the protonated amine surface density were +0.150, +0.169, and +0.108 #/nm^2 for pH 4, 7, and 10, respectively, somewhat consistent with the amine portion of the surface became less positive with higher pH values. Hybrid particles clearly had lower amine surface densities than the APTES-SiO$_2$ particles.

3.6 Concluding Remarks

PSA were successfully synthesized in the sub-100nm range by controlling the citrate concentration. At charge ratio of 1, PSA hydrodynamic diameter was found to be ~40nm. Higher R ratio resulted in larger hydrodynamic diameter. Silicic acid added to PSA produced silicified silica/polymer NP with similar diameter to the PSA. The silica/polymer NPs were broadly dispersed at all tested charge ratio. With the TEM images and line profile analysis, the synthesized NPs were porous and retained DI water up to 25% of their weight. TGA measurement determined that these hybrid NPs were thermally stable up to 800°C similar to bare silica mesoparticles. Surface charge density

analysis showed that silica hybrid particle has a lower aminated density compared to APTES-SiO$_2$ particles.

3.7. References

1.   Murthy, V.S., R.K. Rana, and M.S. Wong, *Nanoparticle-Assembled Capsule Synthesis: Formation of Colloidal Polyamine–Salt Intermediates.* The Journal of Physical Chemistry B, 2006. **110**(51): p. 25619-25627.

2.   Hunter, R.J., *Foundations of Colloids Science.* 2001, New York: Oxford University Press.

3.   Yu, J., et al., *Self-assembly synthesis, tumor cell targeting, and photothermal capabilities of antibody-coated indocyanine green nanocapsules.* J Am Chem Soc, 2010. **132**(6): p. 1929-38.

4.   Rana, R.K., et al., *Nanoparticle Self-Assembly of Hierarchically Ordered Microcapsule Structures.* Advanced Materials, 2005. **17**(9): p. 1145-1150.

5.   Bagaria, H.G., S.B. Kadali, and M.S. Wong, *Shell Thickness Control of Nanoparticle/Polymer Assembled Microcapsules.* Chemistry of Materials, 2010. **23**(2): p. 301-308.

6.   Hildenbrand, M., ed. *Silicic Acid Transport and Its Control* Biomineralization, ed. E. Bauerlein. 2000, Wiley-VCH: Weinheim, FRG. 171-188.

7.   Bergna, H.E. and W.O. Roberts, eds. *Colloidal Silica: Fundamentals and Applications.* Surfactant Science. 2006, CRC Press.

8.   Bauerlein, E., *Biomineralization: progress in biology, molecular biology and application.* 2nd ed. 2004: Wiley-VCH.

9.   Kröger, N., et al., *Species-specific polyamines from diatoms control silica morphology.* Proceedings of the National Academy of Sciences, 2000. **97**(26): p. 14133-14138.

10.   Kroger, N. and M. Sumper, eds. *The Biochemistry of Silica Formation in Diatoms.* ed. E. Bauerlein. 2000, Wiley-VCH: Weinheim, FRG. 151-170.

11.   Compton, S.J. and C.G. Jones, *Mechanism of dye response and interference in the Bradford protein assay.* Analytical Biochemistry, 1985. **151**(2): p. 369-374.

12.   Georgiou, C., et al., *Mechanism of Coomassie brilliant blue G-250 binding to proteins: a hydrophobic assay for nanogram quantities of proteins.* Analytical and Bioanalytical Chemistry, 2008. **391**(1): p. 391-403.

13.   Nagy, L.E., *Alcohol: methods and protocols.* 2008: Humana Press.

14.   Noel, S., et al., *Quantification of Primary Amine Groups Available for Subsequent Biofunctionalization of Polymer Surfaces.* Bioconjugate Chemistry, 2011: p. null-null.

15.   Chial, H.J., H.B. Thompson, and A.G. Splittgerber, *A Spectral Study of the Charge Forms of Coomassie Blue G.* Analytical Biochemistry, 1993. **209**(2): p. 258-266.

16.   Hosokawa, M., *Nanoparticle technology handbook.* 2007: Elsevier.

17.   Ganachaud, F., S. Boileau, and B. Boury, *Silicon Based Polymers: Advances in Synthesis and Supramolecular Organization.* 2008: Springer.

18.   Lefaux, C.J., et al., *Polyelectrolyte spin assembly: Influence of ionic strength on the growth of multilayered thin films.* Journal of Polymer Science Part B: Polymer Physics, 2004. **42**(19): p. 3654-3666.

19.   Moon, J.H., et al., *Absolute Surface Density of the Amine Group of the Aminosilylated Thin Layers: Ultraviolet-Visible Spectroscopy, Second Harmonic*

Generation, and Synchrotron-Radiation Photoelectron Spectroscopy Study. Langmuir, 1997. **13**(16): p. 4305-4310.

Chapter 4

Conclusion

A simple method to synthesize cationically charged, sub-100-nm silica NPs without the use of aminoalkylsilanes was presented. The polymer-salt aggregate assembly chemistry was developed to generate polyallylamine-citrate aggregates in the sub-100-nm size range, by determining the appropriate charge ratio values and precursor concentrations. These aggregates formed silica/polymer hybrid NPs after contacting the aggregate suspension with a silicic acid solution. These NPs did not dis-assemble at high salinity, unlike the parent polymer-salt aggregates. Whether the NPs were measured in the wet state or in dried state, the unimodal particle sizes correlated with the polymer-salt aggregate sizes. This hybrid NPs were mostly inorganic by weight, and the polymer was located throughout the particle interior as well as on the particle surface. The NPs had pzc, zeta potential, and surface charge density values between those of bare SiO_2 particles and amine-functionalized ones, which may prove useful in pH-sensitive applications.

Chapter 5

Future Work

5.1 Introduction

Silica hybrid nanoparticles are a versatile material that can be used safely in biological applications or further modified for other usages. In this section, several applications for silica hybrid nanoparticles are proprosed for future research. This material can be combined with metallic nanoparticles for catalysis or capped with metals to form nanoshells for thermal treatment. In addition, during the course of this study, hollow silica nanoparticles (with polymer-salt aggregates as the core and silica-hybrid as the shell) were also detected. This core-shell structure is a suitable candidate for drug delivery as a nanocapsule allowing bacteria or virus to easily intake the capsule.[1-3] These proposed future works will be discussed in this chapter.

5.2 Core-Shell Structure of Silica Hybrid

The experimental method reported in Chapter 2 yielded mostly solid silica hybrid nanoparticles. However, some nanoparticles were hollow which can be used as nanocapsules for biomedical applications such as drug delivery. Throughout the study, most of the TEM images taken show silica hybrid nanoparticles with a consistent gray shade as seen in Figure 5-1. However, on several occasions, the silica hybrid nanoparticles do not have a consistent gray throughout the particle (see Fig. 5-3). The

inner core has a lighter gray shade compared to the outer edge indicating a hollow interior.
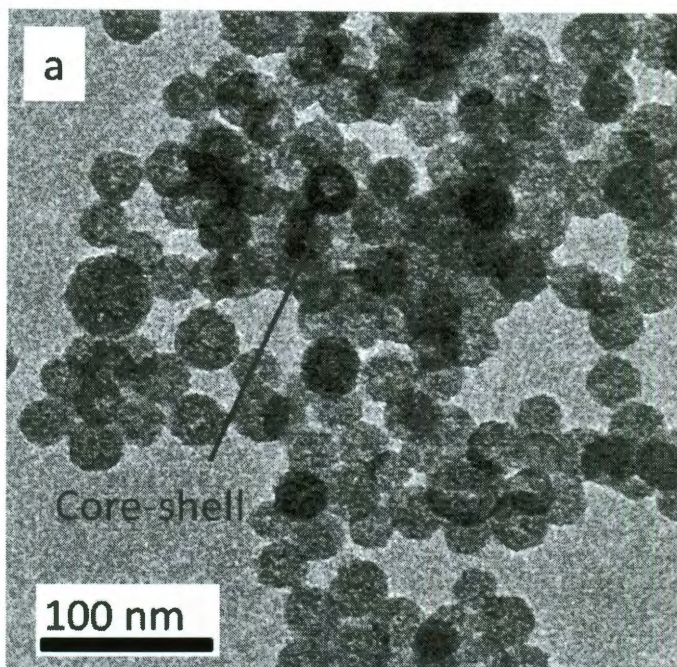
Figure 5-1. TEM image showed a) silica hybrid nanoparticles with consistent gray throughout except 1 particle that can be seen clearly with a lighter shade in the core than the edge.

One of the possible explanations for the formation of the core-shell structure is due to rapid hydrolysis of the silica precursor. The silica precursor (TMOS in HCl) was assumed to hydrolyze into 2-3 nm silica NPs and diffuse into the polymer salt aggregate. There is a possibility that the deposition of 2-3 nm silica NPs occurred rapidly on the surface, preventing further diffusion into the center. To test this hypothesis, two parameters can be changed to control the shell thickness: silicic acid concentration and silicification time. Silicic acid concentration was shown to have an effect on controlling the shell thickness.[4] In addition, changing the silicification time can limit amount of

silicic acid diffusion into the polymer-salt aggregate. These works have not been done but can be easily explored.

5.3 Silica Hybrid as a Catalysis Support

Silica has proven to be an ideal candidate as a support for catalytically active metallic nanoparticles due to its mechanical strength, thermal stability, high surface area, and irreducibility.[5, 6] For example, Au nanoparticles deposited on silica support has been widely used for catalytic oxidation of carbon monoxide (CO)[7, 8] and hydrogen (H_2) to produce hydrogen peroxide (H_2O_2).[9] To test the possibility of using silica hybrid nanoparticles as a support, negatively charged gold nanoparticles were added to a suspension of silica hybrid nanoparticles at pH 3, when silica hybrid NPs have a positive surface charge, to see if it would electrostatically bind to the surface. For this preliminary study, an excess amount of 2-3 nm gold nanoparticles synthesized by the Duff method was added to ensure that maximum adsorption of Au particles.[10] The gold-on-silica hybrid (Au/silica/PAH) nanoparticles suspension was centrifuged to remove excess, unbound gold nanoparticles. TEM was used to image the resulting Au/silica/PAH to prove the attachment of gold NPs on surface. With prior knowledge that gold would appear darker in images due to its higher electron density compared to SiO_2, Figure 5-1 shows that Au particles are attracted to the surface of SiO_2 and remain on the surface even after centrifugation process described above. Gold NPs are spaced out on the surface of silica/PAH NPs with minimal gold clusters formation, resulting in maximum gold surface area for catalytic reactions.
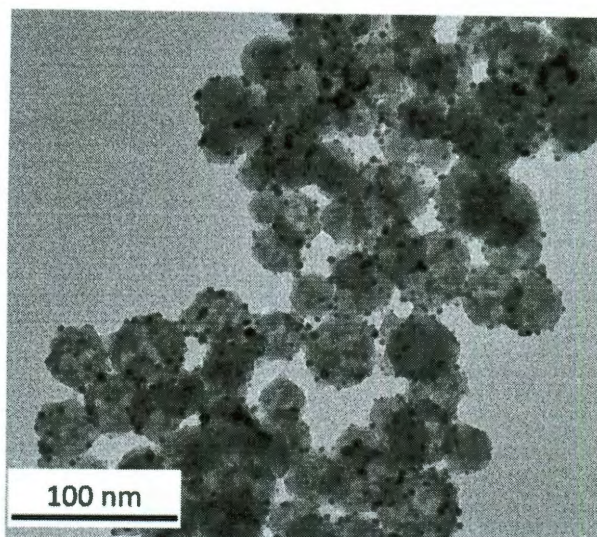
Figure 5-2. Au nanoparticles deposited onto SiO_2. The distribution of Au particles is uniform on silica hybrid particle surfaces.

5.4 Silica-Hybrid as Core for Metallic Nanoshell

Metallic nanoshells have unique electronic property that can be used for thermal treatment, sensors, or used as a surface for surface enhanced Raman spectroscopy (SERS).[11-14] Gold is used widely for the mentioned applications due to its plasmonic and inert properties. The conventional method to synthesize gold nanoshell is to start with a silica core using the Stöber method.[15] The silica particles are then functionalized with APTES to change the surface group of silica nanoparticles from –OH to –NH_2 for easier attraction to negatively charged gold nanoparticles. The addition of Duff gold nanoparticles covers approximately 30% of the surface of silica particle.[10] To form a complete shell, gold salt is added and reduced by CO or formaldehyde.[16, 17] The gold salt continually deposits on the surface of gold nanoparticles and eventually merges to form a complete shell. Figure 5-2 shows preliminary TEM images of

53

unsuccessful nanoshell synthesis using silica hybrid as the core. Since silica/PAH NP has surface amine groups, the functionalization step in the conventional method to make nanoshell unnecessary. The rest of the experimental method is the same as above. Fig 5-2a shows cluster of particles rather than individual particles and Fig. 5-2b has many unbounded gold NPs from self-nucleation during the reduction gold salt.
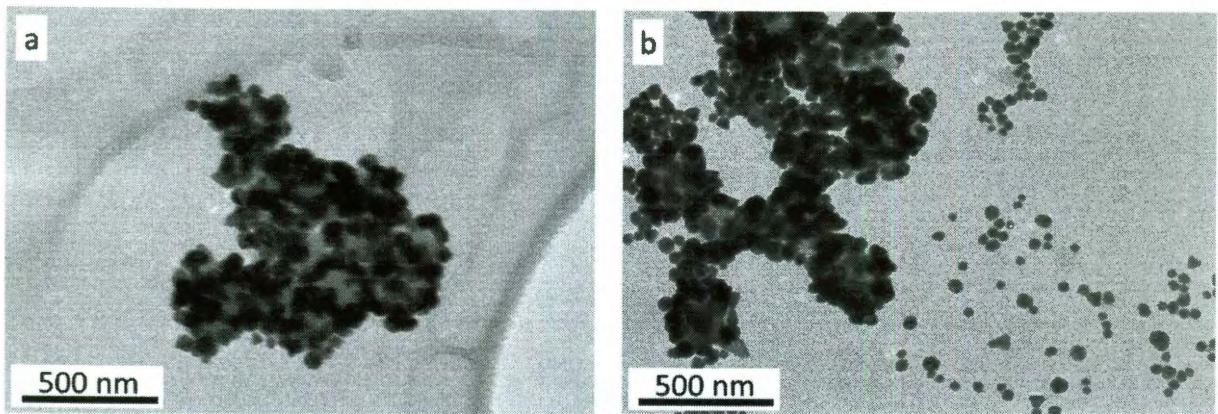

Figure 5-3. a) TEM images of cluster of silica-hybrid with gold nanoparticles on the surface. b) Gold salt reduction also leads to nucleation of gold nanoparticles.

Silica hybrid would provide a good base for gold nanoshell synthesis because of the availability of the amine-groups of the surface. These amine groups provide anchor points for gold nanoparticles. Synthesis of gold nanoshell using silica-hybrid as a core involves a similar step to making Au/SiO_2 catalyst. Using the Au/SiO_2 catalyst as the core, gold salt is added and further reduced using CO method.[16] However, preliminary trials for the synthesis of gold nanoshells did not yield complete shell formation. Also seen were aggregation of silica-hybrid NPs with bound gold NPs on the surface and numerous unbounded gold nanoparticles indicating insufficient surface coverage of gold NPs. To make better shells using silica hybrid as the base, more Duff gold nanoparticles need to be on the surface. One experimental parameter to attract more Duff gold NPs

54

onto the silica/PAH NP surface is to control the pH, which was not done here. As seen in Chapter 3, the pH value changes the surface charge density of the silica/PAH NP. With a higher positively charged surface, more negatively charged gold NPs will get attracted to the surface.

5.5 Gold Nanoshells

The reason for the synthesis of nanoshell structure, which consists of a dielectric core and a metallic shell, is its plasmonics properties enable a wide variety of applications such as biomolecular sensor, thermal treatment of tumors, or surface for chemical analysis (i.e, surface enhanced Raman spectroscopy - SERS, surface enhanced infrared absorption-reflectance - SEIRA).[11, 13, 14, 17, 18] Gold nanoshells were not successfully synthesized using silica hybrid cores less amine coverage on the surface for the attachment of gold. Gold nanoshells were experimented by the author to study chemical reactions.

5.5.1 Chemical Reactions using Gold Nanoshells

Understanding and proving chemicals reactions through measurement has been the holy grail for scientific understanding. Microscopic level studies provide fundamental understanding of adsorption on surfaces and reaction mechanism of catalytic activities. Surface enhanced Raman Spectroscopy has been recently found to have high sensitivity and is promising tool to study chemical reactions.[14] With the field re-energized by Shuming and Nie, SERS is found to be able to have sensitivities up to 10^{14}.[18] The range of surfaces that is suitable for SERS is not limited to roughen metallic films, it now

includes nanoparticles[19], nanostars[20], nanoshells[17], or nanogaps[21]. These surfaces are all in research stage but nanoshells proved to be the most promising material because of thickness controllability, large scale synthesis, and has higher enhancement compared to gold nanoparticles. Heck et al. showed Raman spectroscopic study of the hydrodechlorination of dichloroethane in aqueous solution using gold nanoshells as substrates.[14] Knowing that AuNS can be used to study hydrodechlorination reaction of trichloroethylene (TCE), it would be interesting to use this tool to study other involving chemical reaction such as chloroform hydrodechlorination. Chloroform hydrodechlorination is an interesting reaction because it is listed at a higher priority than TCE.[22]

5.5.2 Materials

The following materials are required for the synthesis of gold nanoshells: gold (III) chloride trihydrate ($HAuCl_4 \cdot 3H_2O$), tetrakis(hydroxymethyl)phosphonium chloride (THPC, 80 wt% in H_2O), aminopropyltriethoxysilane (APTES), polydiallyldimethylammonium chloride (MW 100K, 35 wt% in H_2O), K_2CO_3, NaOH, NaCl, ethanol (180 and 200 proof), were acquired from Sigma Aldrich and silica cores from Precision Colloids (NanoSol120). Palladium precursor is palladium (II) chloride acquired was also acquired from Sigma Aldrich. The catalyst used, which is Pd-Au/Alumina (Au 0.4 wt%, Pd 0.09 wt%), was acquired from Mintek Corp. Deionized water (DIW) was provided by Barnstead Nanopure Diamond System (18.2MΩ) and used in all solutions.

5.5.3 Gold Nanoshell Synthesis

Gold nanoshells are chosen as material for substrate because it can be easily synthesized, has high enhancement, and can be easily tuned to laser frequency for maximum detections. The method to synthesized gold nanoshells was previously described.[16] Briefly, 120nm silica nanoparticles are functionalized with APTES. These functionalized cores are placed into an excess amount of gold nanoparticle solution and left overnight for surface decoration. These seeded silica cores provide smoother surface and uniform shell growth. Duff covered cores are mixed with a potassium carbonate solution of gold chloride. Carbon monoxide was bubbled into the solution for 20s to reduce the gold chloride. As gold salt reduce onto the gold seeds, the islands become larger and merge together to form a complete shell. After the nanoshells were formed, the solution was concentrated by centrifuging at 800 rpm for 30min.

5.5.4 SERS Substrate Preparation

Gold nanoshells are then immobilized onto silicon substrate for SERS analysis. Silicon substrates are first plasma cleaned (Harrick Plasma Cleaner/Sterilizer, PDC-32G) for 5 minutes. Immediately, 30uL of PDDA (polydiallyldimethylammonium, 5% wt.) in ethanolic solution was drop onto the substrate where the droplet was held together by surface tension. The PDDA was left for 15 minutes and thesubstrates were washed off with DI water. Approximately 30uL of concentrated gold nanoshells solution were dropped onto the PDDA functionalized Si wafers and left for 4 hrs for self-assembly. The excess nanoshells were washed off with DI water. For best results, the substrate should be used immediately after immobilization onto Si wafers.

5.5.5 Raman Spectroscopy Measurement

Raman spectra were recorded using InVia Raman Microscope with a 785nm laser and 40x Nikon optic. Laser power was set at 0.05mW and integration time of 10s totaling to scan time of 1 minute per spectrum. The SERS substrate was placed into a closed chamber (Warner Instruments RC-43, 273 uL volume) with one outlet and one inlet. Before each run, with 5mL of N_2 saturated DI water in a 5mL syringe, 3mL was injected through the inlet port. The focus after water injection was tweaked and stabilized for 30 minutes. Other solutions (H2 water, chloroform with various H2 concentrations, and chloroform with N2) were injected in the similar fashion to achieve a complete flush of inner chamber volume. The chloroform concentration used for all experiments were 0.503mM or 60 ppm. Raman spectra were recorded continuously for a period of time, which is depending on the reaction.

5.5.6 Raman Spectra of Chloroform Hydrodechlorination

Chloroform hydrodechlorination was first studied by checking activities using Raman spectroscopy with saturated concentration of N_2 and H_2. When adding in chloroform in N2 saturated water at T = 0min, the Raman bands shift back and forth, however no significant thing can be detected on the surface. As soon as chloroform and H2 is added to the reaction chamber at T=25 min, increasing Raman activities were seen with a significant amount of CF chemisorb onto the surface (Figure x a). The red in the plots signified high intensities and blue are minimal activities. If we reverse the sequence and

flush with just hydrogen at the end, chloroform was removed off the surface from decreasing intensity (red/yellow to blue) (Figure x b). Since the concentration of chloroform is high, many vibrational bonds are enhanced from the gold surface resulting in overlapping bands. The significant increase in all bands is detrimental to this experiment since individual bonds cannot be extracted for interpretation. Hydrogen amount was lowered to see if reaction can be held on the nanoshell surface for interpretation.
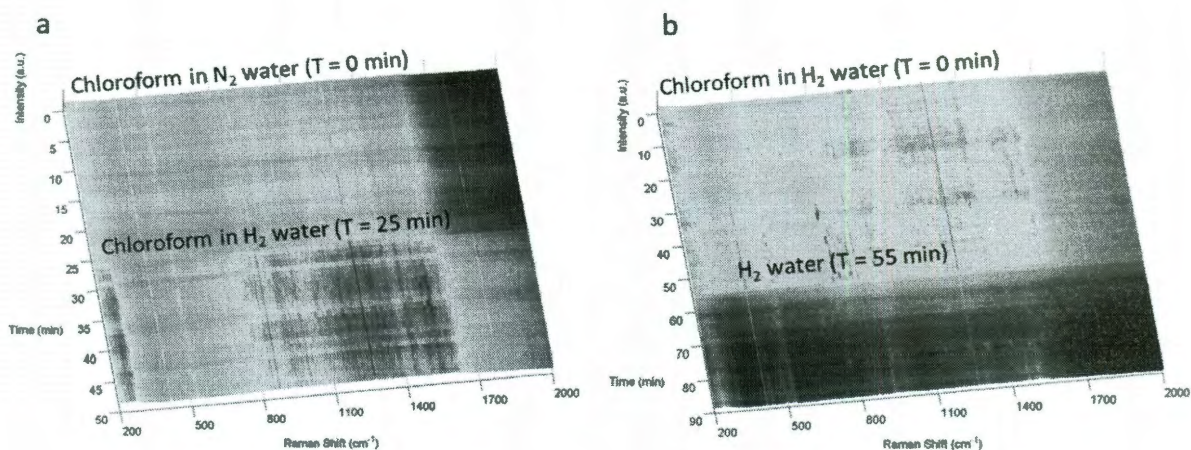

Figure 5-4. Raman spectra of chloroform a) adsorption to and b) desorption from the gold nanoshell surface. Chloroform concentration is 0.503 mM or 60 ppm with saturated amount of specified gas.

In order to restrict the amount of hydrogen, H_2 saturated DI water was first purged into the cell. During this particular step, an undetermined amount of hydrogen adsorbed onto the gold nanoshell surface. When N2 saturated water was purged into the reaction chamber, minimal activities were detected on the gold nanoshell surface. The majority of

the reaction was seen when chloroform was introduced into the system. Limiting the amount of hydrogen prevented rapid hydrodechlorination, therefore spectra of activities are held on the surface longer as seen in Figure x from T = 60-80min. These spectra provided a multitude of informations in which can be extracted to prove the reaction mechanism. These works required much more analysis but these initial Raman spectroscopic measurements proved that gold nanoshells is a useful material for SERS. Gold nanoshell surface is not a good catalytic surface for hydrodechlorination reaction, however it is a good surface for spectroscopic studies of hydrodechlorination reaction since it slows down the activities long enough for Raman scan by the instrument.
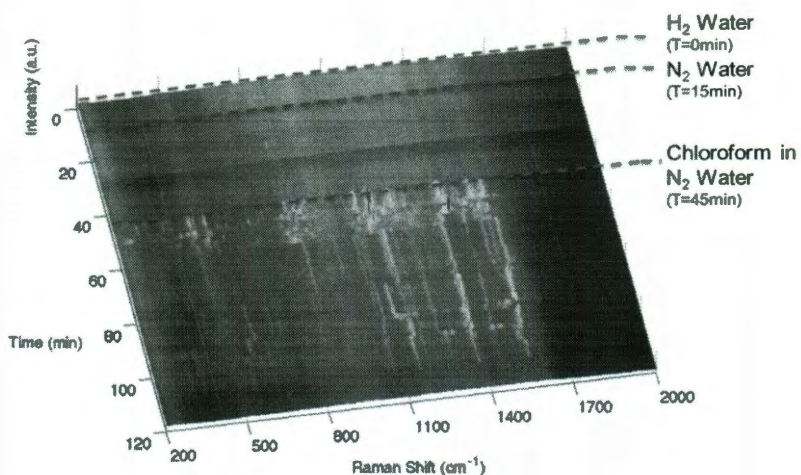

Figure 5-5. Raman spectra recorded over a period of 2 hrs of chloroform activities on gold nanoshell surface. H2 saturated water was introduced initially at T= 0min, followed by introduction of N2 saturated water (T = 15min), and chloroform in N2 saturated water at T = 45 min.

5.6 References

1. Underhill, R.S., et al., *Oil-Filled Silica Nanocapsules for Lipophilic Drug Uptake: Implications for Drug Detoxification Therapy.* Chemistry of Materials, 2002. **14**(12): p. 4919-4925.

2. Liu, Y., H. Miyoshi, and M. Nakamura, *Novel drug delivery system of hollow mesoporous silica nanocapsules with thin shells: Preparation and fluorescein isothiocyanate (FITC) release kinetics.* Colloids and Surfaces B: Biointerfaces, 2007. **58**(2): p. 180-187.

3. Chen, H., et al., *Porous Silica Nanocapsules and Nanospheres: Dynamic Self-Assembly Synthesis and Application in Controlled Release.* Chemistry of Materials, 2008. **20**(18): p. 5894-5900.

4. Bagaria, H.G., S.B. Kadali, and M.S. Wong, *Shell Thickness Control of Nanoparticle/Polymer Assembled Microcapsules.* Chemistry of Materials, 2010. **23**(2): p. 301-308.

5. B. Cornils, W.A.H., R. Schlogl, C.H. Wang, ed. *Catalysis from A to Z: A Concise Encyclopedia.* 2000, Wiley-VCH: Weinheim.

6. Z. Ma, F.Z., R.B. King, ed. *Encyclopedia of Inorganic Chemistry, 2nd Edition.* 2005, John Wiley & Sons: Chichester. 1768.

7. Lin, S.D., M. Bollinger, and M.A. Vannice, *Low temperature CO oxidation over Au/TiO2 and Au/SiO2 catalysts.* Catalysis Letters, 1993. **17**(3): p. 245-262.

8. Okumura, M., et al., *Chemical vapor deposition of gold on Al2O3, SiO2, and TiO2 for the oxidation of CO and of H2.* Catalysis Letters, 1998. **51**(1-2): p. 53-58.

9. Ishihara, T., et al., *Synthesis of hydrogen peroxide by direct oxidation of H2 with O2 on Au/SiO2 catalyst.* Applied Catalysis A: General, 2005. **291**(1-2): p. 215-221.

10. Duff, D.G., A. Baiker, and P.P. Edwards, *A new hydrosol of gold clusters. 1. Formation and particle size variation.* Langmuir, 1993. **9**(9): p. 2301-2309.

11. Lal, S., S.E. Clare, and N.J. Halas, *Nanoshell-Enabled Photothermal Cancer Therapy: Impending Clinical Impact.* Accounts of Chemical Research, 2008. **41**(12): p. 1842-1851.

12. Raschke, G., et al., *Gold Nanoshells Improve Single Nanoparticle Molecular Sensors.* Nano Letters, 2004. **4**(10): p. 1853-1857.

13. Kundu, J., et al., *Surface enhanced infrared absorption (SEIRA) spectroscopy on nanoshell aggregate substrates.* Chemical Physics Letters, 2008. **452**(1-3): p. 115-119.

14. Heck, K.N., et al., *Observing Metal-Catalyzed Chemical Reactions in Situ Using Surface-Enhanced Raman Spectroscopy on Pd—Au Nanoshells.* Journal of the American Chemical Society, 2008. **130**(49): p. 16592-16600.

15. Stöber, W., A. Fink, and E. Bohn, *Controlled growth of monodisperse silica spheres in the micron size range.* Journal of Colloid and Interface Science, 1968. **26**(1): p. 62-69.

16. Brinson, B.E., et al., *Nanoshells Made Easy: Improving Au Layer Growth on Nanoparticle Surfaces.* Langmuir, 2008. **24**(24): p. 14166-14171.

17.   Oldenburg, S.J., et al., *Nanoengineering of optical resonances.* Chemical Physics Letters, 1998. **288**(2-4): p. 243-247.

18.   Nie, S. and S.R. Emory, *Probing Single Molecules and Single Nanoparticles by Surface-Enhanced Raman Scattering.* Science, 1997. **275**(5303): p. 1102-1106.

19.   Doering, W.E. and S. Nie, *Single-Molecule and Single-Nanoparticle SERS: Examining the Roles of Surface Active Sites and Chemical Enhancement.* The Journal of Physical Chemistry B, 2001. **106**(2): p. 311-317.

20.   Hao, F., et al., *Plasmon Resonances of a Gold Nanostar.* Nano Letters, 2007. **7**(3): p. 729-732.

21.   Lim, D.-K., et al., *Nanogap-engineerable Raman-active nanodumbbells for single-molecule detection.* Nat Mater, 2010. **9**(1): p. 60-67.

22.   CDC, *CERCLA Priority List of Hazardous Substances*, A.f.T.S.D. Registry, Editor. 2009: Atlanta, GA. p. http://www.atsdr.cdc.gov/cercla/05list.html.